University of Alberta

Investigating Interactions between Cellulose Nanocrystals (CNCs)

and Proteins

by

Cong Cao

A thesis submitted to the Faculty of Graduate Studies and Research
in partial fulfillment of the requirements for the degree of

Master of Science

Department of Chemistry

To my parents and my boyfriend, Yang

Abstract

Cellulose nanocrystals (CNCs) are an emerging renewable and sustainable nanomaterial which has received increasing attention. They are abundant, non-toxic, biodegradable and chemically inert. CNCs have unique characteristics not met by traditional cellulose-derived materials, leading to investigations/applications of CNC's across all disciplines. The objective of this work is to investigate interactions of proteins with CNC's by atomic force microscopy (AFM) and spectroscopic techniques. Results indicated an electrostatic driven interaction that depends on incubation time, protein concentration and protein intrinsic properties such as molecular weight, charge distribution and iso-electric point. Understanding CNC-protein interactions aids in the development of new biosensing platforms that utilize green-material substrates. The usefulness of a CNC surface as a substrate for immunoassays was developed and evaluated by surface plasmon resonance (SPR). CNC films were shown to provide a suitable platform for antibody immobilization and antigen binding, with LOD's comparable to other SPR based biosensors.

List of Tables

List of Figures

List of Abbreviations

AFM	Atomic Force Microscopy
anti-g-IgG	Goat IgG Antibody
BMA	Butyl Methacrylate
BSA	Bovine Serum Albumin
CNC	Cellulose Nanocrystal
CTAB	Cetyl Trimethylammonium Bromide
dPAA	Phenylacetic Acid Diazonium Salt
EA	Ethyl Acrylate
EDC	1-Ethyl-3-(3-dimethylaminopropyl) Carbodiimide
FG	Fibrinogen
g-IgG	Goat IgG Antigen
HOPG	Highly Ordered Pyrolytic Graphite
IgG	Immunoglobulin G
IRRAS	Infrared Reflection Absorption Spectroscopy
LBL	Layer-by-layer
LOD	Limit of Detection
LYZ	Lysozyme
MMA	Methyl Methacrylate
MUAM	Mercaptoundecylamine Hydrochloride
$NaH_2PO_4 \cdot H_2O$	Sodium Phosphate, Monobasic
NaOH	Sodium Hydroxide
NHS	N-hydroxysuccinimide

PB	Phosphate Buffer
PDDAC	Poly(diallyldimethylammonium chloride)
pI	Iso-electric Point
PPF	Pyrolyzed Photoresist Films
RMS	Root Mean Square
RPM	Rotation per Minute
SPR	Surface Plasmon Resonance
-PLL	-Poly-L-lysine

List of Symbols

% R	Change in Reflectivity
[C]	Concentration
°	Degree
A	Absorbance
a.u.	AbsorbanceUnits
Ar	Argon
Au	Gold
C	Celsius
cm	Centimeter
Cr	Chromium
h	Hour
I_p	Intensity of p-polarized Light
I_s	Intensity of s-polarized Light
K	Kelvin
K_{ads}	Adsorption Constant
K_d	Dissociation Constant
M	Molar
min	Minute
ml	Milliliter
M	MegaOhm
N	Newton
nm	Nanometer

nM	Nanomolar
Pa	Pascal
Si	Silicon
wt	Weight
Δ% R	Change in Percent Reflectivity in Difference Image
θ	Angle of Incidence
μg	Microgram
μl	Microliter
μM	Micromolar
μm	Micrometer
$\nu_{C\text{-}O}$	Frequency of C–O stretch
$\nu_{O\text{-}H}$	Frequency of O–H stretch
σ_{blank}	Standard Deviation of Blank

Chapter 1 Introduction

1.1 General Overview and Research Objective

Industries and customers are increasingly demanding products made from renewable and sustainable resources which are biodegradable, non-petroleum based, environmentally friendly, and have minimal safety or health risks. [1] Natural cellulose based materials, such as wood, cotton, hemp and so forth have served our society for thousands of years. Even today their use in construction products, textiles, paper, etc. plays a key role in worldwide industries. However, as science and technology evolve, the demands of functionality, durability and uniformity which will be required for the new generation of cellulose based products cannot be met with traditional cellulosic materials. Fortunately, cellulose nanoparticle is a base fundamental reinforcement unit used to strengthen all subsequent structures within plants, algae, and some marine creatures. By extracting cellulose to the nanoscale, a new cellulose based "building block" is available for new biopolymer composites.[1]

Cellulose nanocrystals (CNCs) are an ideal material that has been intensely studied by researchers.[2-6] CNC possesses many unique structural and mechanical properties. For example, CNCs have a high aspect ratio, low density (1.566 g·cm^{-3}), and a reactive surface consisting of -OH side groups which can be used to functionalize the CNC surface to achieve different

surface properties.[7, 8] In addition, CNCs have a greater axial elastic modulus than Kevlar and its mechanical properties are within the range of other reinforcement materials.[9] Due to these unique chemical and mechanical properties, a wide range of potential applications include barrier films[10], transparent films[11], antimicrobial films[12], flexible displays[13], biomedical implants[14], reinforcing fillers for polymers[15], pharmaceuticals[16], fibers and textiles[17], drug delivery[18], batteries[19], electroactive polymers[20] and supercapacitors[21].

Our interest is in the development of applications of CNC films. In this thesis I focus on investigating the interactions between CNC films and proteins, and the application of CNC films as a platform surface chemistry for biosensing.

A dense CNC film will provide a high-surface area substrate and the polysaccharide based structure of CNCs can potentially resist non-specific adsorption of proteins. However, since the CNC surface bears negative charges, proteins can adsorb to CNC surfaces through electrostatic forces. The use of CNC films for biosensing applications will follow from a thorough understanding of protein adsorption. Understanding CNC-protein interactions will be of significant importance to develop new CNC applications in bio-sensing platforms that utilize green-material substrates.

1.2 Cellulose Nanocrystals

Cellulose is the world's most abundant biopolymer and is the structure backbone of all plants. Tunicate is the only animal known to produce cellulose microfibrils as the mantle. In 1838, Anselme Payen first suggested that the cell walls of a large number of plants consist of the same fibrous material, to which he gave the name "cellulose".[22] Since then the structure, properties and applications of cellulose have been intensely studied.[2-7]

Cellulose is a linear polymer consisting of D-anhydroglucose units $(C_6H_{10}O_5)_n$, where n is dependent on the cellulose source material, and has a flat ribbon-like conformation. The two adjacent anhydroglucose molecules compose a repeating unit (Figure 1.01 A). The glucose units are linked together through an oxygen covalently bonded to C1 of one glucose ring and C4 of the adjoining ring and is termed a β-1,4-glycosidic bond.[7] Hydroxyl groups and oxygens of the adjoining ring molecules also interact via H-bonding resulting in strong intrachain interactions. The anhydroglucose units do not lie exactly in plane, but assume a chair conformation, with successive glucose residues rotated through an angle of 180° about the molecular axis.[23]

(A)

(B) **Multiple cellulose chains form elementary fibrils**

Amorphous

Crystalline

(C) **CNCs are extracted through acid hydrolysis**

Cellulose nanocrystals
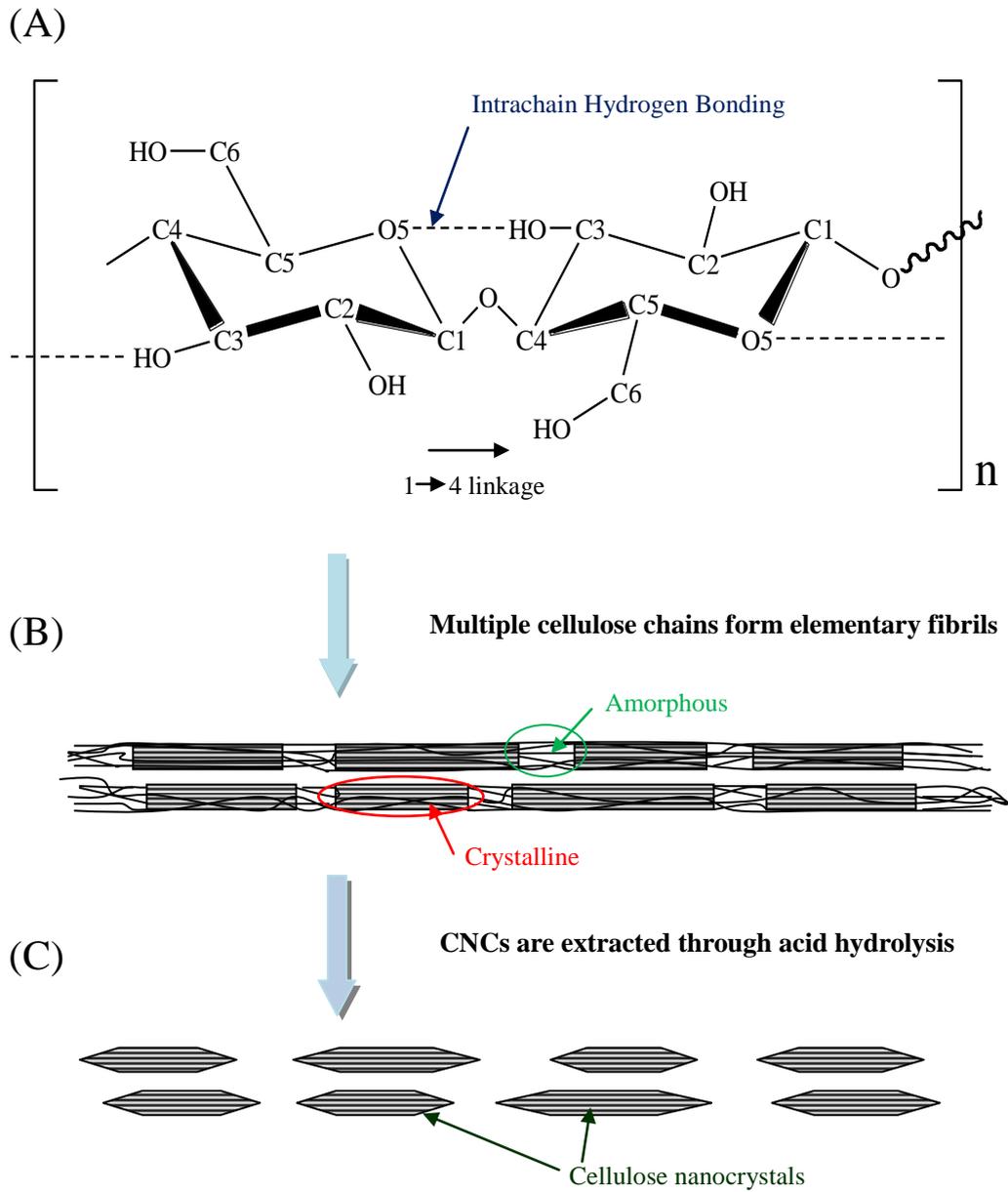
Figure 1.01. Schematics of (A) single cellulose chain repeating unit, showing the intrachain hydrogen bonding and 1→4 linkage directionality, (B) idealized elementary fibrils formed by multiple cellulose chains, showing one of the suggested amorphous and crystalline regions, (C) cellulose nanocrystal after acid hydrolysis selectively dissolved the amorphous regions.

Intermolecular hydrogen bonding as well as van der Waals forces promote parallel stacking of multiple cellulose chains to form elementary fibrils, which are usually considered to be the lowest level of hierarchy in cellulose assembly (Figure 1.01 B).[24] Hydroxyl groups of the chain surfaces make the surface hydrophilic, and also result in hydrogen bonding interactions between adjacent fibrils. These elementary fibrils aggregate into larger microfibrils which are 5–50 nm in diameter and several microns in length, containing 2–30,000 cellulose molecules in their cross-section.[1] Microfibrils further aggregate into larger fibril bundles and finally to plant fibers.[25] The intra- and inter-chain hydrogen bonding network discussed above brings about the linear configuration and relative stability in cellulose.

There are several polymorphs of crystalline cellulose, which are cellulose I, II, III and IV. The polymorphs differ in terms of the orientation and geometry of the cellulose chains within the respective unit cells. The two most common forms are the natural cellulose I and the regenerated cellulose II. Our work focuses on the cellulose I structure, which is the crystalline cellulose with the highest axial elastic modulus.[26] It is naturally produced by a variety of organisms, such as trees, plants, algae, tunicates, and bacteria. So it is also referred to as "natural" cellulose.

Cellulose fibrils are the main reinforcement phase for plants, trees, tunicates, algae, and bacteria, but are not uniformly crystalline. There are regions within these cellulose fibrils where the cellulose chains are arranged in

a highly ordered (crystalline) structure distributed throughout the material, as well as regions which are disordered (amorphous). As shown in Figure 1.01 C, the crystalline regions can be extracted from microfibrils through acid hydrolysis (acid treatment) during which the amorphous regions are selectively hydrolyzed.[5, 6, 27] The resulting rod-like nanoparticles are called cellulose nanocrystals (CNCs) or nanocrystalline cellulose (NCC). They are typically 3–5 nm wide and 50–500 nm in length.[28] Sulphuric acid is the most commonly used acid in the extraction process and results in a CNC surface populated with sulfate ester groups. Thus, an important characteristic of CNCs is its negative surface charge. Hence CNCs disperse well in water.

Due to their abundance, high stiffness and strength, low density and biodegradability, CNCs serve as promising candidates for the preparation and applications in the field of materials science. One of the applications is the CNC co-deposition with functional polymers or other nanoparticles. A straightforward method is using the layer-by-layer (LBL) approach with polymers or metallic nanoparticles having an opposite surface charge to the CNCs. The co-deposit of TiO_2 with CNCs can be used to create open porous structures with metallic nanoparticles, without loss of conductivity throughout the film. [29] This approach is also very effective and versatile using CNCs bearing negatively charged sulfate surface groups and positively charged poly(diallyldimethylammonium chloride) (PDDAC)[30] and chitosan[31]. In another work, MacLachlan and coworkers developed a photonic, mesoporous,

inorganic (silica) solid which is a cast of a chiral nematic liquid crystal formed from nanocrystalline cellulose.[32] The material can be used as hard templates to synthesize a variety of new materials with chiral nematic structures that have hitherto been inaccessible.

CNCs also have many potential applications in pharmaceutical and biomedical fields due to their bioactivity, biocompatibility, biodegradability and low-toxicity. CNCs were introduced as a suitable excipient in the preparation of pharmaceutical acrylic beads based on an ethyl acrylate (EA), methyl methacrylate (MMA) and butyl methacrylate (BMA) mixture matrix.[33] The presence of CNCs, functionalized as a co-stabilizer, reduced the bead size and induced a narrower size distribution of beads. In another work, Mangalam *et al.* reported the synthetic protocols for grafting DNA to CNCs and subsequent duplex formation to form bonded structures.[34] The study sets the stage for further work to develop DNA/CNC hybrid materials for specific applications. Jackson *et al.* investigated the controlled release effect of CNCs with the surface modification using the cationic surfactant cetyl trimethylammonium bromide (CTAB) on the drug molecules.[35] It was shown that the surface modification on CNCs increased the zeta potential from -55 to 0 mV in a concentration-dependent manner. The CTAB-modified CNCs can bind significantly with non-ionized hydrophobic anticancer drug molecules, which exhibited the release profile in a controlled manner over a 2-day period.

1.3 Protein Adsorption

Protein adsorption onto solid surfaces is of significance in various applications. For example, immobilization of proteins is one of key steps in surface-based immunoassay methods and biosensors.[36] Another example is for drug storage, where protein adsorption should be prevented. Adsorption of therapeutic protein onto container walls may result in denaturation, inactivation of the drug, as well as change of the overall bulk concentration.[37] In all of these applications, a fundamental understanding of interactions between proteins and solid surfaces is required.

Proteins are biomolecules which are composed of amino acid subunits, which form the primary structure of proteins. It is the unique combination of amino acids that gives a protein its properties. Each amino acid has a side chain. The interaction between the side chains results in localized folding, making the linear sequence into regular structure motifs such as α helices and β sheets, which are the proteins' secondary structure. Folding of the regions between α helices and β sheets generates the tertiary protein structure, making the proteins compact and intact. The driving forces behind the tertiary folding are mainly from non-covalent interactions such as hydrogen bonding, van der Waals forces and electrostatic interactions. The interior region of proteins is usually hydrophobic whilst the external surface is occupied by hydrophilic charged group. The charged groups gain or lose charges depending on the pH of the surrounding environment, as well as its own individual polar/nonpolar

qualities. The charge of proteins is determined by the pK_a values of their amino acid side chains and the terminal amino acids. The net charge of the protein is determined by the sum charge of its constituents, resulting in electrophoretic migration in a physiologic electric field. The iso-electric point (pI) is the pH at which a particular molecule or surface carries no net electrical charge or the negative and positive charges are equal. At a pH above their pI they carry a net negative charge; below their pI, proteins carry a net positive charge. Charged regions of proteins can greatly contribute to the interactions with other molecules and surfaces, as well as their own tertiary structure (protein folding).

As a result of hydrophilicity, charged amino acids tend to be located on the outside of proteins, where they are able to interact with surfaces, making proteins intrinsically surface active.[38-42] Protein adsorption is a critical phenomenon which describes the aggregation of these molecules on the exterior of a material. The tendency for proteins to adsorb and remain attached to a surface depends on intrinsic properties of proteins, such as protein size, charge, structure, and various other chemical properties. It is also related to the material properties like surface energy and charge distribution. For example, larger proteins have a higher tendency to adsorb and remain on a surface due to the increased number of contact sites between the amino acids and the surface. In addition, when the net charge of the protein is opposite to the surface charge, the protein may bind to the surface more readily.

Protein in solution

Diffusion

Conformation change   Conformation change
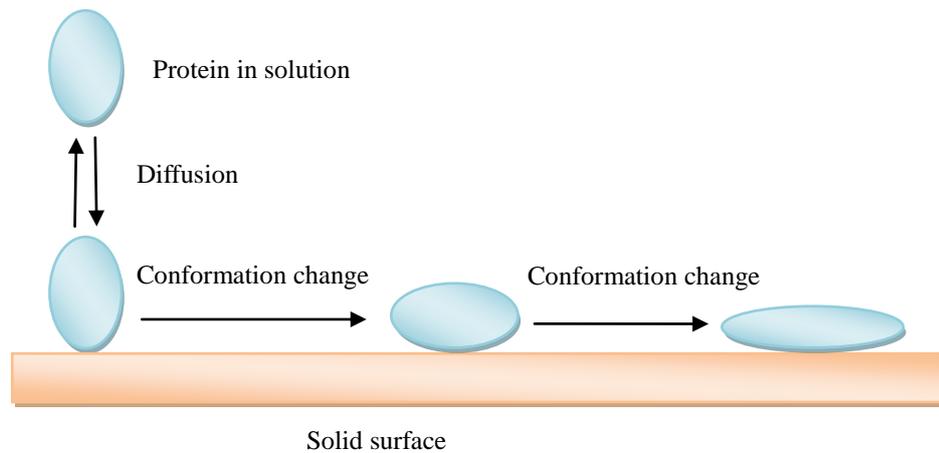
Solid surface

Figure 1.02. A representation showing possible steps involved with protein adsorption to solid surfaces. Longer time and surface with greater hydrophobicity incite greater conformation change.[42]

Protein adsorption to a surface can be viewed as a collection of events, which is shown in Figure 1.02.[42] In order for proteins to adsorb, they must first come into contact with the surface from the bulk solution to a surface through one or some of these major transport mechanisms: diffusion, bulk flow, and thermal convection. Under conditions of low flow and minimal temperature gradients, the adsorption process is mainly a result of diffusion. Then, a relaxation and attachment process occurs to optimize the interaction between the protein and surface. Proteins during this process may unfold to some extent in order to increase the surface affinity by increasing the contact area. This causes partial structure rearrangement of a protein or even complete protein denaturation. Longer time and surfaces with greater hydrophobicity

incite greater conformation change. In most of the cases, protein adsorption has been found to be an irreversible process under physiological conditions. Yet the proteins may detach from the surface through an exchange mechanism depending on the extent of relaxation.[43, 44] Desorption can also occur by the variation of pH or the addition of surfactants. Some of the major driving forces behind protein adsorption include: surface energy, hydrophobicity, intermolecular forces, and ionic or electrostatic interactions. Understanding protein adsorption is of importance in biomedical, medical, industrial and environmental applications.

1.4 Plasma Proteins

The plasma proteins utilized for experiments presented in the following chapters are bovine fibrinogen (BFG), bovine serum albumin (BSA), chicken lysozyme (LYZ), and immunoglobulin (IgG). Plasma proteins can be found circulating in blood, and each of them has different functions. My research interest is mainly focused on investigating the electrostatic driven interaction between proteins and CNC film surface, so an important reason that these proteins are chosen is the wide range of their iso-electric points and different charges distributed throughout different proteins. The molecular weights, iso-electric points and charges under physiological pH (pH=7.4) of the four proteins are listed in Table 1.1.

Fibrinogen has been extensively studied recently due to its key

component in blood coagulation (thrombosis) resulted from the conversion from fibrinogen to fibrin by the enzyme of thrombin. The fibrin monomers aggregate, preventing blood loss. Fibrinogen is a soluble, and relatively large dimeric glycoprotein (MW=340 kDa). The structure of fibrinogen is illustrated in Figure 1.03 A. It consists of two sets of three intertwined polypeptide chains. Each contains one Aα, Bβ and γ chain in one of the dimers, and the two halves are linked at N-termini by 29 disulfide bonds.[45, 46] Fibrinogen contains four major domains, including two outer D domains, a central E domain and an αC domain, with each having different chemical properties. The D and E domains are more hydrophobic than the αC domain. The overall charge of fibrinogen at physiological pH (pH 7.4) is -10.[46] Among the four domains, the D and E domains are negatively charged, whilst the αC domain bears net positive charges on it. Due to its large size and heterogeneous charge distribution, fibrinogen is very surface active and is capable of adsorbing to various materials.

Albumin is one of the most abundant proteins in serum or plasma and is often used as a passivating agent to prevent the adhesion of cells. The main function of albumin is to transport fatty acid molecules which exhibit low solubility in aqueous environments. Bovine serum albumin (BSA) is a serum albumin protein derived from cows. With a molecular weight of 66,210 Daltons, BSA is a globular monomeric protein consisting of 607 amino acid groups.[47] As shown in Figure 1.03 B, it contains three domains (I, II and III),

which fold into a heart-shaped structure according to NMR[48] and X-ray crystallography characterization[49]. BSA has a dimension of approximately 3 nm × 9 nm, with 35 cysteinyl residues, 34 of which participate in 17 disulfide bridges. The iso-electric point of BSA is 4.7, and it has an overall charge of -18 at physiological pH.[50] With the change of pH values, BSA has been found to undergo reversible conformation changes. Due to the flexibility in its structure and hydrophobic interactions, BSA has the ability to adsorb onto a variety of materials and has been commonly used as the blocking protein on surfaces to prevent non-specific binding.

Lysozyme (LYZ) is an enzyme protein which can be found abundantly in egg white and in a number of secretions, such as tears, saliva and human milk. LYZ can inhibit bacterial growth by breaking down the bacterial wall in mammals. X-ray studies have identified that LYZ is a small spherical, yet hard and rigid protein with molecular weight of approximately 14.5 kDa.[51] As shown in Figure 1.03 C, lysozyme is composed of 129 amino acids and forms a single polypeptide chain, with a dimension of 14 nm × 9 nm × 4 nm. The iso-electric point of LYZ is approximately positive 11.0, therefore it is a cationic protein at pH 7.4. LYZ is usually used as a model in studies of electrostatic driven adsorption of proteins to surfaces.

(A)

D domain   E domain   D domain

Coiled-coil Connectors

(B)

Domain I

Domain III

Domain II

(C)

(D)

Light Chain

Binding Site

Binding Site

Variable Region

Constant Region

Heavy Chain
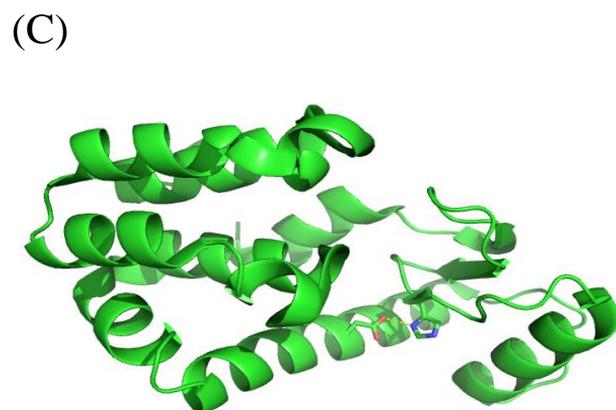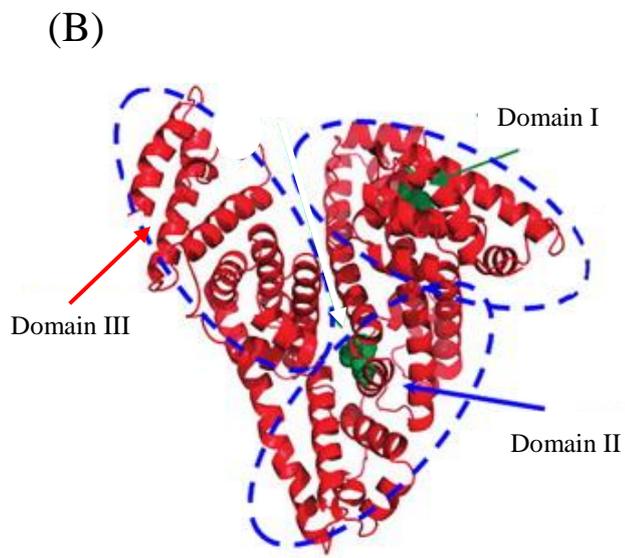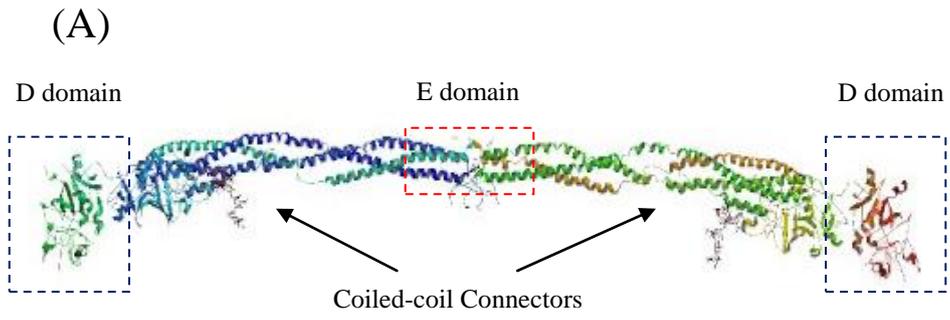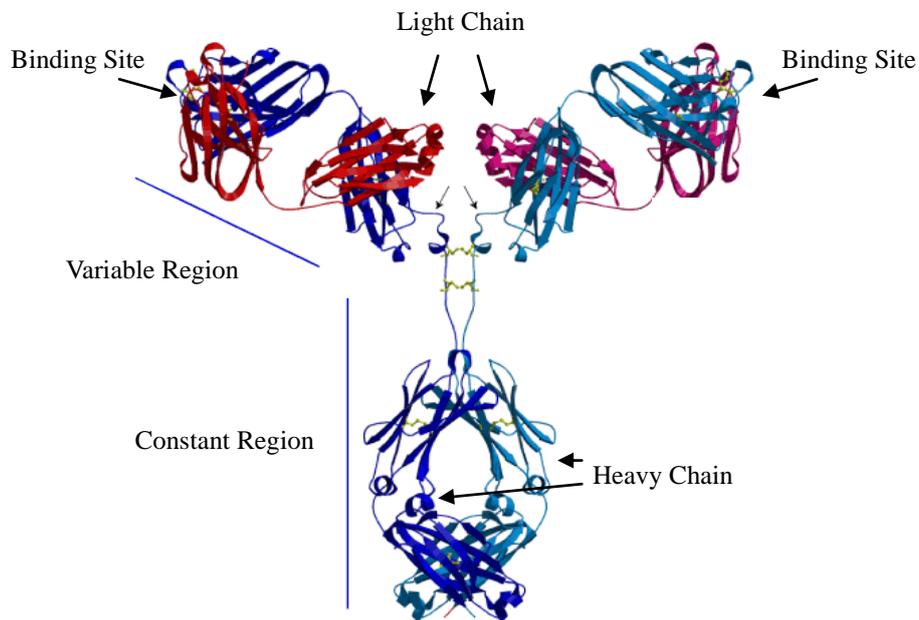
Figure 1.03. (A) Structure of fibrinogen (MW ～340 kDa). Fibrinogen is a

dimer, containing three domains (D, E and αC). Dimension of fibrinogen is ～47 nm

in length and 4-6 nm of thickness. (B) Structure of bovine serum albumin (MW ～66

kDa). Single peptide consists of three domains (I, II and III), and folds into a heart-

shape structure. Dimensions are ～3 nm × 9 nm. (C) Structure of lysozyme (MW～

14.5 kDa). Dimensions are ～14 nm × 9 nm × 4 nm. (D) Structure of an IgG antibody

(MW～150 kDa) containing the constant region in the "stem" and the variable region

in the "forks". The specificity of binding is due to the composition of the variable

regions.

Immunoglobulin G (IgG) is an antibody complex, which is a major component of the immune system response to foreign substances (antigens). IgG is the antibody isotype mainly found in blood and extracellular fluid. IgG protects the body from infection by binding many kinds of pathogens, such as viruses, bacteria and fungi. Representing approximately 75% of the serum immunoglobulins in humans, IgG is the most abundant antibody isotype found in circulation.[52] IgG antibodies are relatively large molecules with a molecular weight of about 150 kDa. As shown in Figure 1.03 D, it has a tetrameric quaternary structure, containing two identical heavy chains of about 50 kDa and two identical light chains of about 25 kDa. The two heavy chains are linked to each other and to an adjacent light chain by disulfide bonds. The resulting tetramer has two identical halves, forming a Y-shape structure. Each end of the fork contains an identical antigen binding site.

Table 1.1. Summary of molecular weight, iso-electric point and charge at pH=7.4 of proteins studied.

Protein	Molecular Weight (kDa)	Iso-electric Point (pI)	Charge at pH=7.4
Fibrinogen (FG)	340	4.5-5.0	-10
Bovine Serum Albumin (BSA)	66	4.7	-18
Lysozyme (LYZ)	14.5	11.0	+7.5
Immunoglobulin (IgG)	150	6.5-8.5[53]	/

1.5 Surface-based Immunoassays and Surface Plasmon Resonance (SPR)

An immunoassay is a biochemical test that measures the presence or concentration of a macromolecule through the use of an antibody or immunoglobulin. Immunoassays rely on the ability of an antibody to recognize and bind specifically to a target. In immunology the biomolecule bound by an antibody is referred to as an antigen. In our study, the immunoassay uses an antigen to detect for the presence of antibodies. Rosalyn Sussman Yalow and Solomon Berson are credited with the development of the first immunoassays in the 1950s. Since then, immunoassays have gained popularity and become a powerful tool in the development of biosensors [54], clinical diagnosis[55], environmental analysis[56] and the food industry[57]. Biomolecular interactions and detection at solid surfaces are of significance in the rapidly growing field of biosensors. The surface based immunoassay begins with the immobilization of probe molecules, such as an antibody or an antigen, onto a pretreated surface. Target molecules (complementary antigen or antibody) in a solution interact with and physisorb to the probe molecules on surface. Surfaces act as the communication link between the protein species and facilitate our understanding of the interfacial behavior of proteins. The use of surfaces in protein-protein studies has led to a number of immunoassay sensing platforms and the proliferation of detection methodologies. Our aim is to develop a new CNC-based biosensing platform that utilizes a green material substrate.
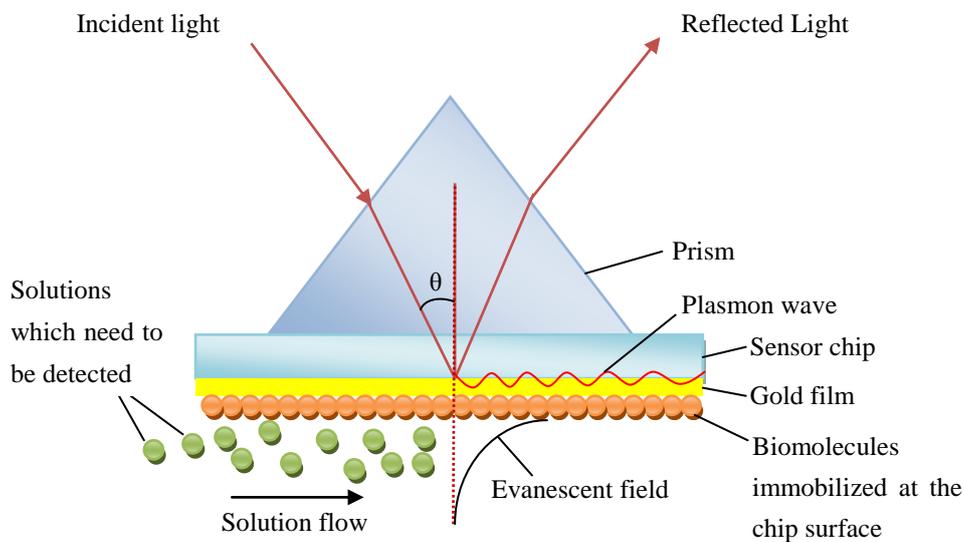
Figure 1.04. Schematic of the surface plasmon resonance (SPR) biosensor. At a specific angle (θ), the surface Plasmon creates an evanescent wave that decays into the solution at the sensor surface leading to a minimum in reflected light intensity.

Surface plasmon resonance (SPR) is a commonly used, label-free optical biosensing technology.[58-60] As shown in Figure 1.04, SPR uses a sensor chip consisting of a thin (e.g. 50 nm) layer of gold on a glass surface. The receptors can be attached to the gold surface and a liquid containing the analyte flows over the binding surface. The SPR method is based on optical measurement of refractive index changes associated with the binding of the analyte molecules in a sample to biorecognize molecules immobilized on the SPR sensor. The detection system consists of a polarized light beam that passes through a prism on top of the glass layer. The light is totally reflected but another component

of the wave called an evanescent wave, couples into the gold layer, where it can excite electrons at the gold surface. At the correct wavelength and angle (θ), plasmon resonance, which is a resonance wave of excited electrons, is produced at the gold surface, decreasing the total intensity of the reflected optical wave. The observed SPR signal is related to the molecule's mass and the affinity of the interaction. Adsorption of molecules onto the gold surface changes the interfacial dielectric constant (reflective index) and changes the conditions of plasmon resonance. The intensity, angle or wavelength of the reflected light can all be measured to provide information on biomolecule adsorption. Since the late 1990's, SPR biosensors have become the main tool for the study of biomolecular interactions both in life science and pharmaceutical research. In addition, they have been increasingly applied in the detection of chemical and biological substances in important areas such as medical diagnostics, environmental monitoring, and food safety and security.

1.6 Atomic Force Microscopy (AFM)

Atomic force microscopy, one of the foremost tools for imaging, measuring and manipulating matter, has become a popular technique in observing the dynamic events in protein adsorption process at the molecular level. AFM has enjoyed widespread applications in protein research, ranging from imaging of individual proteins [61, 62] to the analysis of protein films [63-66]. AFM possesses several characteristics that make it an attractive tool in

examining protein adhesion to surfaces. Firstly, as the surface does not need to be conductive, fixed, or dyed, minimal surface preparation is necessary prior to imaging with AFM, which makes imaging ease and rapidity. Additionally, in imaging mode, AFM has a high resolution which approaches nanometer resolution[67], which is comparable to or even better than electron microscopy. Thus, Atomic force microscopy in principle enables direct observation of the real-space topography for detecting the spatial distribution of adsorbed proteins.[68] In addition, AFM can be performed in either air or liquid, collecting images and force data acquired for fully hydrated surfaces *in situ*.

As displayed in Figure 1.05, an AFM consists of a cantilever with a sharp tip (probe) at its end, which is used to scan the sample surface. When the tip is brought into proximity to the surface, a deflection of the cantilever occurs due to the forces between the tip and the sample. Typically, the cantilever deflection is measured by a laser beam reflected from the cantilever top onto an array of position-sensitive photodiodes.

Depending on the application, AFM can be operated in a number of modes. In general, possible imaging modes are divided into static, also called contact mode and a variety of dynamic (non-contact or AC) modes where the cantilever is oscillated. Both the contact and AC modes are used in the work presented in the following chapters.
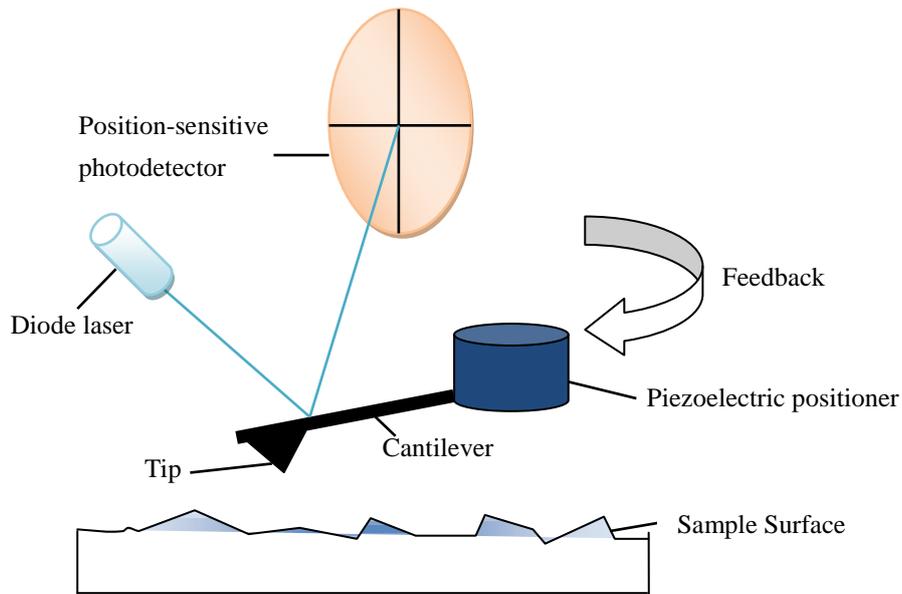
Figure 1.05. General schematic of the atomic force microscope (AFM).

In static mode, the cantilever is "dragged" across the surface of the sample and the deflection of the cantilever is used to measure the contours of the surface. This technique is also called contact mode. The force between the tip and the surface is kept constant during scanning by lowering or raising the sample. The magnitude of the feedback signal which is used to keep the force constant is proportional to the topography of the surface.[69] In contact mode, the tip is close to the surface of the sample, where attractive forces can be quite strong, causing the tip to "snap-in" to the surface and damage the sample surface. [70] Thus contact mode AFM is always done where the overall force is repulsive. In addition, the scratching technique can be performed under

contact mode to measure the thickness of a film. In scratching, the tip is scanned under strong loading forces to remove the substance film from the substrate in a well-defined way, leaving behind deep trenches with the characteristic shape of the plough used. By measuring the height difference between the bottom point of the trench and the top point of the original film surface, the thickness of the substance film can be obtained.

In tapping mode, also called AC mode, the cantilever is driven to oscillate at approximately its resonance frequency by a small piezoelectric element mounted in the AFM tip holder. An electronic servo uses the piezoelectric actuator to adjust the height of the cantilever above the sample, in order to maintain a set cantilever oscillation amplitude as the cantilever is scanned over the sample. A tapping AFM image is therefore produced by imaging the force of the intermittent contacts of the tip with the sample surface. Changes in topography correspond to changes in the amplitude of the oscillation, while changes in sample stiffness are represented by changes in the oscillation's phase lag. This method of tapping significantly lessens the damage done to the surface and the tip. However, as opposed to contact mode, little lateral forces to the substrate are observed via AC mode, though the vertical forces may be large, which possibly leads to altering the height of soft samples. [71]

Topography images provide two-dimensional information about the surface chemistry of proteins. However, tip contamination, sample damage and thermal drift in the image are still fundamental problems to be solved.

1.7 Infrared Reflection Absorption Spectroscopy (IRRAS)

Besides AFM, infrared reflection absorption spectroscopy (IRRAS) is another powerful method to identify and characterize the molecular structure of adsorbates on metal surfaces, such as chain conformation and orientation. In IRRAS, light impinges onto the sample surface at a well defined and controlled angle of incidence. Metal surface constrains the observed incident radiation and dipole orientation. Incident radiation interacts with adsorbates and then reflects from the metal surface. The reflected light is detected at an angle equal to the angle of incidence. Only the perpendicular component of incident radiation contributes to the observed signal, and only the dipole moments with a contribution along the surface normal interact with the incident radiation. The technique measurements provide frequencies and intensities of molecular vibrations accompanied by changing molecular dipole moments. The vibrational frequencies that are detected can be interpreted in terms of molecular conformation. By monitoring the vibrational characteristics of the peptide backbone (C=O and N-H) stretches, proteins and peptides that are adsorbed to surfaces can be qualitatively and quantitatively determined by IRRAS.[69, 72]The ease and rapidity of aquiring high quality spectra from small amount of proteins make IRRAS suitable for the work presented in this thesis.

1.8 Motivations and Intentions

It has been reported in the literature that molecular layers of polysaccharides significantly inhibit the non-specific adsorption of proteins.[73] A dense CNC film will provide a high-surface area substrate and the polysaccharide based structure of CNCs can potentially resist non-specific adsorption of proteins, which is our motivation to explore the protein adsorption behavior on CNC films in Chapter 2. IRRAS and ATM are utilized to investigate the interactions between CNC films and proteins.

In the biosensing area, the motivation was to design a simple and readily available platform that utilizes cellulose nanocrystals, which is a green-material substrate, to analyze antibody-antigen binding. In Chapter 3 this idea is explored using IRRAS and applied to an immunoassay detected by SPR.

1.9 References

1. Moon, R. J.; Martini, A.; Nairn, J.; Simonsen, J.; Youngblood, J. *Chemical Society Reviews* **2011**, *40*, 3941–3994.

2. Elazzouzi-Hafraoui, S. Nishiyama, Y.; Putaux, J. L.; Heux, L.; Dubreuil, F.; Rochas, C. *Biomacromolecules* **2008**, *9*, 57–65.

3. De Rodriguez, N. L. G. W.; Thielemans, W.; Dufresne, A. *Cellulose* **2006**, *13*, 261–270.

4. Habibi, Y.; Hoeger, I. S.; Kelley, S.; Rojas, O. J. *Langmuir* **2010**, *26*, 990–1001.

5. Beck-Candanedo, S.; Roman, M.; Gray, D. G. *Biomacromolecules*, **2005**, *6*, 1048–1054.

6. Bai, W.; Holbery, J.; Li, K. C. *Cellulose* **2009**, *16*, 455–465.

7. Samir, M. A. S. A.; Alloin, F.; Dufresne, A. *Biomacromolecules* **2005**, *6*, 612–626.

8. Lahiji, R. R.; Xu, X.; Reifenberger, R.; Raman, A.; Rudie, A.; Moon, R. J. *Langmuir* **2010**, *26*, 4480–4488.

9. Ishikawa, A. Okano, T. Sugiyama, *Journal of Polymer* Science **1997**, *38*,463–468.

10. Saxena, A.; Elder, T. J.; Kenvin, J.; Ragauskas, A. J. *Nano-Micro Letters* **2010**, *2(4)*, 235–241.

11. Nogi, M.; Iwamoto, S.; Nakagaito, A. N.; Yano, H. *Advanced Materials* **2009**, *21*, 1595–1598.

12. Andresen, M.; Stenstad, P.; Møretrø, T.; Langsrud, S.; Syverud, K.; Johansson, L.; Stenius, P. *Biomacromolecules* **2007,** *8*, 2149–2155.

13. Okahisa, Y.; Yoshida, A.; Miyaguchi, S.; Yano, H. *Composites Science and Technology* **2009**, *69*, 1958–1961.

14. Macocinschi, D.; Filip, D.; Vlad, S.; Butnaru, M.; Knieling, L. *International Journal of Biological Macromolecules* **2013**, *52*, 32–37.

15. Boldizar, A.; Klason, C.; Kubát, J.; Näslund, P.; Sáha, P. *International Journal of Polymeric Materials and Polymeric Biomaterials* **1987**, *11(4)*, 229–262.

16. Sievens-Figueroa, L.; Bhakay, A.; Jerez-Rozo, J. I.; Pandya, N.; Romañach, R. J.; Michniak-Kohn, B.; Iqbal, Z.; Bilgili, E.; Davé, R. N. *International Journal of Pharmaceutics* **2012**, *423(2)*, 496–508.

17. Roland, J. C.; Mosiniak, M.; Roland, D. *Acta Botanica Gallica* **1995**, *142(5)*, 463–484.

18. Dash, R.; Ragauskas, A. J. *RSC Advances* **2012**, *2*, 3403–3409.

19. Jabbour, L.; Gerbaldi, C.; Chaussy, D.; Zeno, E.; Bodoardo, S.; Beneventi, D. *Journal of Materials Chemistry* **2010**, *20*, 7344–7347.

20. Cai, Z.; Kim, J. *Journal of Applied Polymer Science* **2008**, *109*, 3689–3695.

21. Wang, H.; Zhu, E.; Yang, J.; Zhou, P.; Sun, D.; Tang, W. *Journal of Physical Chemistry C*, **2012**, *116 (24)*, 13013–13019.

22. Payen, A. *Comptes Rendus Hebdomadaires des Seances de l Academie des Sciences* **1838**, *7*, 1052–1056.

23. Eichhorn, S. J.; Baillie, C. A.; Zafeiropoulos, N.; Mwaikambo, L. Y.; Ansell, M. P.; Dufresne, A.; Entwistle, K. M.; Herrera-Franco, P. J.; Escamilla, G. C.; Groom, L.; Hughes, M.; Hill, C.; Rials, T. G.; Wild, P.M. *Journal of Materials Science* **2001**, *36*, 2107–2131.

24. Klemm, D.; Heublein, B.; Fink, H.-P.; Bohn, A. *Angewandte Chemie International Edition* **2005**, *44*, 3358–3393.

25. Klemm, D.; Kramer, F.; Moritz, S.; Lindstrom, T.; Ankerfors, M.; Gray, D.; Dorris, A. *Angewandte Chemie International Edition* **2011**, *50*, 5438−5466.

26. Ishikawa, A.; Okano, T.; Sugiyama, J. *Polymer* **1997**, *38*, 463–468.

27. De Rodriguez, N. L. G.; Thielemans, W.; Dufresne, A. *Cellulose* **2006**, *13*, 261–270.

28. Elazzouzi-Hafraoui, S.; Nishiyama, Y.; Putaux, J. L.; Heux, L.; Dubreuil, F.; Rochas, C. *Biomacromolecules,* **2008**, *9*, 57–65.

29. Bonne, M. J.; Milsom, E. V.; Helton, M.; Thielemans, W.; Wilkins, S.; Marken, F. *Electrochemistry Communications* **2007**, *9* (8), 1985–1990.

30. Bonne, M. J.; Edler, K. J.; Buchanan, J. G.; Wolverson, D.; Psillakis, E.; Helton, M.; Thielemans, W.; Marken, F. *Journal of Physical Chemistry C* **2008**, *112* (7), 2660–2666.

31. Tsourounaki, K.; Bonne, M. J.; Thielemans, W.; Psillakis, E.; Helton, M.; McKee, A.; Marken, F. *Electroanalysis* **2008**, *20* (22), 2395–2402.

32. Shopsowitz, K. E.; Qi, H.; Hamad, W. Y.; MacLachlan, M. J. *Nature* **2010**, *468*, 422–426.

33. Villanova, J. C. O.; Ayres, E.; Carvalho, S. M.; Patrício, P. S.; Pereira, F. V.; Oréfice, R. L. *European Journal of Pharmaceutical Sciences* **2011**, *42*, 406– 415.

34. Mangalam, A. P.; Simonsen, J.; Benight, A. S. *Biomacromolecules* **2009**, *10,* 497–504.

35. Jackson, J. K.; Letchford, K.; Wasserman, B. Z.; Ye, L.; Hamad, W. Y.; Burt, H. M. *International Journal of Nanomedicine* **2011**, *6*, 321–330.

36. Benmakroha, Y.; Zhang, S.; Rolfe, P. *Medical and Biological Engineering and Computing* **1995***, 33,* 811–821.

37. Brange, J.; Langkaer, L. (1993) Insulin Structure and Stability in Stability and Characterization of Protein and Peptide Drugs (Wang, Y. J., Pearlman, R., Eds.) p 315, Plenum Press: New York.

38. Gray, J.J. *Current Opinion in Structural Biology* **2004**, *14*, 110–115.

39. Losche, M. *Current Opinion in Biotechnology* **1997***, 2,* 546–556.

40. Ramsden, J. J. *Chemical Society Reviews* **1995**, *24*, 73–78.

41. Haynes, C. A.; Norde, W. *Colloids and Surfaces B: Biointerfaces* **1994**, *2,*517–566.

42. Hlady, V.; Buijs, J. *Current Opinion in Biotechnology* **1996**, *7*, 72–77.

43. Norde, W.; Giacomelli, C. E. *Macromolecular Symposia* **1999**, *145*, 125–136.

44. Vermonden, T.; Giacomelli, C. E.; Norde, W. *Langmiur,* **2001**, *17*, 3734–3740.

45. P. S. and Marchant, R. E. *Thrombosis and Haemostasis* **1999**, *82*, 1053–1060.

46. Feng, L. and Andrade, J. D. (1995) in Proteins at Interfaces II: Fundamentals and Applications (Horbett, T. A. and Brash, J. L., eds), p. 67, American Chemical Society, Washington, D. C.

47. Peters, T. Jr. (1975) in The Plasma Proteins (Putnam, F. W., ed) 2nd Ed, Vol. 1, pp. 140-142, Academic Press, New York.

48. Bos, O. J. M.; Lowe, C. R. *Journal of Colloid and Interface Science* **1994**, *166*, 102–108.

49. Carter, D. C.; He, X. M.; Munson, S. H.; Twigg, P. D.; Gernert, K. M.; Broom, M. B.; Miller, T. Y. *Science* **1989**, *244*, 1195–1198.

50. Peters, T. J. *Advances in Protein Chemistry* **1985**, *37*, 161–245.

51. Sarmiento, F.; Ruso, J. M.; Prieto, G.; Mosquera, V. *Langmuir* **1998**, *14*, 5725–5729.

52. Unqueira, L. C.; Carneiro, J. (2005) Basic Histology: Text and Atlas. McGraw-Hill, New York.

53. Kane, M. M.; Banks, J. N. (2000) In Immunoassays (Gosling, J. P. ed), chapter 2, pp. 52-53, Oxford University Press, Oxford.

54. Morgan, C. L.; Newman, D. J.; Price, C. P. *Clinical Chemistry* **1996**, *42*, 193–209.

55. Tsikas, D. *Clinica Chimica Acta* **2004**, *344*, 215–217.

56. Lee, J. K.; Ahn, K. C. Stoutamire, D. W.; Gee, S. J.; Hammock, B. D. *Journal of Agricultural and Food Chemistry* **2003**, *51*, 3695–3703.

57. Anand, A.; Moreira, R.; Henry, J.; Chowdhury, M.; Cote G.; Good, T. *Lwt-Food Science and Technology* **2005**, *38*, 849–858.

58. Mullett, W. M.; Lai, E. P. C.; Yeung, J. M. *Methods* **2000**, *22*, 77–91.

59. Kanda, V.; Kariuki, J. K.; Harrison, D. J.; McDermott, M. T. *Analytical Chemistry* **2004**, *76*, 7257–7262.

60. Tian, Y.; Chen, Y. H.; Song, D. Q.; Liu, X.; Bi, S. Y.; Zhou, X.; Cao, Y. B.; Zhang, H. Q. *Analytica Chimica Acta* **2005**, *551*, 98–104.

61. Marchant, R. E.; Barb, M. D.; Shainoff, J. R.; Eppel, S. J.; Wilson, D. L.; Siedlecki, C. A. *Thrombosis and Haemostasis* **1997**, *77*, 1048–1051.

62. Fritz, M.; Radmacher, M.; Cleveland, J. P.; Allersma, M. W.; Stewart, R. J.; Gie selmann, R.; Janmey, P.; Schmidt, C. F.; Hansma, P. K. *Langmuir* **1995**, *11*, 3529–3535.

63. Rasmusson, J. R.; Erlandsson, R.; Salaneck, W. R.; Schott, M.; Clark, D. T.;Lundstrom, I. *Scanning Microscopy* **1994**, *8*, 481–490.

64. Baty, A. M.; leavitt, P. K.; Siedlecki, C. A.; Tyler, B. J.; Suci, P. A.; Marchant, R. E.; Geesey, G. G. *Langmuir* **1997**, *13*, 5702–5710.

65. Ta, T. C.; Sykes, M. T.; McDermott, M. T. *Langmuir* **1998**, *14*, 2435–2443.

66. Gunning, A. P.; Mackie, A. R.; Wilde, P. J.; Morris, V. *Langmuir* **1999**, *15*, 4636–4640.

67. Dufrêne, Y. *Nature Reviews Microbiology* **2008**, *6*, 674–680.

68. Kim, D. T.; Blanch, H. W.; Radke, C. J. *Langmuir* **2002,** *18,* 5841–5850

69. Ta, T. C.; McDermott, M. T. *Analytical Chemistry* **2000**, *72*, 2627–2634.

70. Toscano, A.; Santore, M. M. *Langmuir*, **2006**, *22*, 2588–2597.

71. Abou-Saleh, R. H.; Connell, S. D.; Harrand, R.; Ajjan, R. A.; Mosesson, M. W., Smith, D. A. M.; Grant, P. J.; Ariens, R. A.; *Biophysical Journal* **2009**, *96*, 2415–2427.

72. Liedberg, B.; Ivarsson, B.; Lundstrom, I. *Journal of Biochemical and Biophysical Methods* **1984**, *9*, 233–143.

73. Ratner, D. M.; Adams, E. W.; Su, J.; O'Keefe, B. R.; Mrksich, M.; Seeberger, P. H. *ChemBioChem* **2004**, *5 (3)*, 379–383.

Chapter 2 Investigating Interactions between Cellulose Nanocrystal (CNC) Films and Proteins

2.1 Introduction

Cellulose nanocrystal (CNC) is an emerging nanomaterial that has drawn increasing attention recently.[1-4] It is abundant, sustainable, renewable, and biodegradable. CNCs are highly crystalline (54–88%) rod-like particles, 3–5 nm wide and 50–500 nm in length.[2] They have unique chemical and mechanical characteristics that cannot be met by traditional cellulose-derived materials, such as high aspect ratio, low density, high stiffness, high tensile strength and very low coefficients of thermal expansion.[5] These properties of CNCs are exploited in a variety of different applications in pharmaceuticals[6], fibers and textiles[7], drug delivery[8] and so forth.

CNC films can be used for a variety of applications. For example, a tunable green oxygen barrier through layer-by-layer self-assembly of chitosan and CNCs was reported by Li et al., which holds promise for gas barrier applications in food and drug packaging.[9] In addition, various CNC reinforced nanocomposite films have been intensely studied using CNCs as fillers to improve the strength and stiffness of the resulting composites.[10, 11] Spin coating is a common process to prepare CNC films.[12, 13] Gray and coworkers have reported that a smooth CNC film can be formed through spin coating on mica and used as models to study surface phenomena, where the

effects of surface morphology and roughness are minimized.[14] Besides spin coating, CNC films can also be prepared by Langmuir-Schaefer[15], layer-by-layer[16], casting and evaporating[17] techniques.

Recently researchers have been making efforts in creating and applying paper-based devices that have the capability to detect and/or deactivate biological substances such as bacteria and viruses.[18-20] Paper represents a useful supporting material in developing sensing devices either as a separation medium or as a sample capture and transport media for dipstick assays.[21] Paper is widely used in biosensing devices because it is readily available and inexpensive. In addition, paper wicks aqueous fluids, and this wicking enables passive transport of fluids without active pumping.[18] Printing and coating technologies allow for the application of almost any fluid onto dry paper.[19] The cotton CNCs used in our work originate from Whatman filter paper. They possess some unique mechanical and chemical properties as well as the advantages of ordinary paper. Our ultimate goal is to develop a biosensing platform utilizing the unique structure and properties of CNCs.

Protein adsorption onto solid surfaces is of significance in various applications. For example, immobilization of proteins is one of key steps in surface-based bioassays.[22] For many applications, a fundamental understanding of interactions between proteins and solid surfaces is required. Compared to the receptor-ligand binding, which involves a particular site of the biomolecule, nonspecific adsorption generally involves the interaction of a

fraction of the amino acid sequence with the solid surface. Predefined control over protein adsorption is a prerequisite to rationally design interfaces for biosensors.

This chapter is focused on the formation and characterization of CNC films, and the subsequent exposure of the CNC films to proteins. The CNC film thickness can be controlled by CNC suspension concentration. Furthermore, protein adsorption is shown to be driven by the electrostatic interaction between the CNC film and proteins, which depends on intrinsic properties of the proteins such as size, charge distribution and iso-electric point. A thorough understanding of protein adsorption is the foundation for the use of CNC films in biosensing applications.

2.2 Experimental

2.2.1 Preparation of Gold Substrates

All glass substrates and glassware were cleaned with hot piranha solution (1:3 30% H_2O_2: 98% H_2SO_4) for 15 min, followed by rinsing thoroughly with deionized (18.2 MΩ)/filtered water (NANOpure™ water purification system, Barnstead International, Dubuque, Iowa). Substrates were blown dry using argon gas. 99.99% Au shot (Goodfellow) was used to deposit gold for all substrates via thermal evaporation (Torr International, INC). Substrates consisted of 300 nm gold deposited on glass microscope slides. A layer of Cr (ESPI Metals) with a thickness of 15 nm was deposited in between the glass

slide and the gold film for better adhesion.

2.2.2 Preparation of CNC Films

The gold substrates were first cleaned with UV/ozone treatment for 15 min. Then the gold substrate slides were soaked in an ethanolic solution of 100 μM mercaptoundecylamine hydrochloride (MUAM, $HS–(CH_2)_{11}–NH_2·HCl$) for 24 h, followed by a thorough rinse with anhydrous ethanol to remove unbounded alkanethiolate from the surface. After blown dry with argon, the slides were incubated in 7.5×10^{-3} wt% cotton CNC (purchased from Alberta Innovates Technology Futures, AITF) water suspension for 24 h. The slides were then rinsed thoroughly with deionized (18.2 MΩ) water and dried under argon.

Spin coating is another method for making thicker and smoother CNC films. A 3.0 wt% CNC water suspension was prepared by sonicating for 30 min, followed by filtering through a 0.45 μm membrane to get rid of large agglomerates. Then a series CNC suspensions with different concentrations (0.5 wt%, 1.0 wt% and 2.0 wt%) were made by diluting the stock CNC solution (3 wt%). A volume of 2 ml of each CNC solution was added from a micropipette onto the MUAM modified gold slides and spun at 4000 RPM for 60 seconds using a PWM32 Series Photoresist Spinner (Headway research. Inc., Texas, USA). The samples were heated after spin coating at 120 °C for 1 h to prevent CNCs from redispersing when the slides were wetted.

2.2.3 Protein Adsorption

Phosphate buffer (PB) was prepared with adding 0.1 M sodium hydroxide (NaOH, CALEDON Lab Ltd., Georgetown, ON, Canada) solution drop by drop to 1 mM reagent grade sodium phosphate, monobasic ($NaH_2PO_4 \cdot H_2O$, Sigma, St. Louis, MO), meanwhile measuring the pH of the mixed solution with a pH meter (XL 50, Accumet, Fisher Scientific) until the pH reached 7.40. As the CNCs are sensitive to the ionic strength, the absence of chloride and potassium ions in this lab-made phosphate buffer prevents the aggregation of CNCs when incubating the CNC into protein solutions. Bovine fibrinogen (BFG, Sigma, St. Louis, MO), chicken lysozyme (LYZ, MP Biomedicals, LLC) and bovine serum albumin (BSA, Sigma, St. Louis, MO) were prepared at concentrations of 100 μg/ml in PB. CNC modified slides were immersed in protein solutions for 2 h, followed by rinsing with 1 mM PB to wash off any unbounded protein molecules and blown dry with argon. At this point, the slides were ready for infrared reflection absorption spectroscopy (IRRAS) and atomic force microscopy (AFM) experiments.

2.2.4 Infrared Spectra Measurements

All IRRAS spectra were recorded using a Mattson Infinity Fourier Transform Spectrometer (Madison, WI) equipped with a low noise mercury-cadmium-tellurium (MCT) detector cooled at 77 K by liquid nitrogen. A reflection accessory and a home-built slide holder were housed in an external auxiliary bench. A self-assembled C_{18} thiol monolayer on gold substrate was

used as the background. CNC films on gold slides before and after immersed in BFG, BSA and LYS protein solutions were examined. Spectra were taken using 500 scans at 2 cm^{-1} resolution with a glancing angle of 86°.

2.2.5 Protein Adsorption Isotherms

Gold substrate with MUAM monolayer was immersed in 7.5×10^{-3} wt% cotton CNC solution for 24 hours, followed by thorough rising with DI water and blown dry under argon. A class of protein (BFG, BSA and LYZ) solutions was in advance prepared. 1.000 mg/ml solution was prepared at first with pH=7.4 PB as a stock solution and then diluted to each lower concentration. The concentrations used for protein adsorption isotherm study were 0.005, 0.010, 0.050, 0.100, 0.250, 0.500 mg/ml for each protein. CNC substrates were incubated in protein solution from the lowest concentration to the highest one. The incubation time for each concentration was 1 h. IRRAS was employed to assess the amount of protein adsorption for each individual concentration. The same substrate would be dipped into the next higher concentration of protein solution after one IRRAS spectrum was collected. MUAM self-assembled gold substrates without CNCs were used for the control experiment. The procedure was identical for all the three proteins (BFG, BSA and LYZ).

2.2.6 Atomic Force Microscopy Measurements

AFM images were obtained by MFP3D (Asylum Research Santa Barbara, CA). Igor Pro software (version 6.04) was used for the real-time control and data acquisition functions. Silicon nitrite cantilevers (Olympus AC240TS)

with nominal spring constant of 2 N/m and a nominal resonant frequency of ~70 kHz were used. All AFM measurements were performed under ambient conditions where the humidity and temperature were kept constant at about 20% and 20.8 °C, respectively. Tapping mode (AC mode) was used for topographic imaging. Contact mode was used for film thickness measurement.

2.3 Results and Discussion

2.3.1 Characterization of CNC Films

To characterize CNC films, various techniques can be used. In this study, CNC films on gold substrates were characterized with IRRAS and AFM. Results indicate that the CNC film, formed via physisorption to an amine-terminated SAM on gold, consists of uniform and well packed nanoparticles.

2.3.1.1 IRRAS Spectrum of CNC

CNC nanoparticles bear negative charges on their surface as a result of the sulphate groups created during the sulfuric acid hydrolysis of cellulose fibers. We chose an amine-terminated SAM formed from the adsorption of MUAM to gold as the substrate for CNC films. Since the MUAM SAM interface is positively charged due to a mixture of ammonium and amine terminated groups at pH 7.4, CNC films can be formed via physisorption to the SAM mainly through an electrostatic driven interaction. Immersion in 7.5×10^{-3} wt% cotton CNC solution for 24 h results in CNC adsorption equilibrium onto MUAM SAM. Figure 2.01 shows the IRRAS spectrum of

CNC films adsorbed to the MUAM monolayer on a gold substrate. The region between 900 and 1500 cm^{-1} is displayed in part A, and the region between 3000 and 3600 cm^{-1} is shown in part B.

The schematic of a single cellulose chain repeating unit of CNC is displayed in Figure 2.02 for the band assignment interpretation in Table 2.1. Generally, the bands located in the region 950 – 1200 cm^{-1} are mainly due to the C–O stretch in alcoholic moieties and the cyclic C–O of the acetal O–C–O–C groups. Bands from 3000 to 3600 cm^{-1} are characteristic of O–H stretching modes in alcoholic groups.[24, 25] The C–O stretching band at 1114 cm^{-1} will be used for CNC quantification analysis presented in the following sections because there is a minimal overlap of this absorption peak compared with those of other modes. The position of the band is in good agreement with published data.[27] The peak intensity is directly related to the amount of CNCs bound to amine terminated alkanethiolate surface but cannot be directly quantitated.

(A)

0.001 a.u.

1457
1370
1361
1336
1316
1206
1114
1064
1036
1005
985

Wavenumber (cm^{-1})

(B)

0.001 a.u.

3406
3354
3303

Wavenumber (cm^{-1})
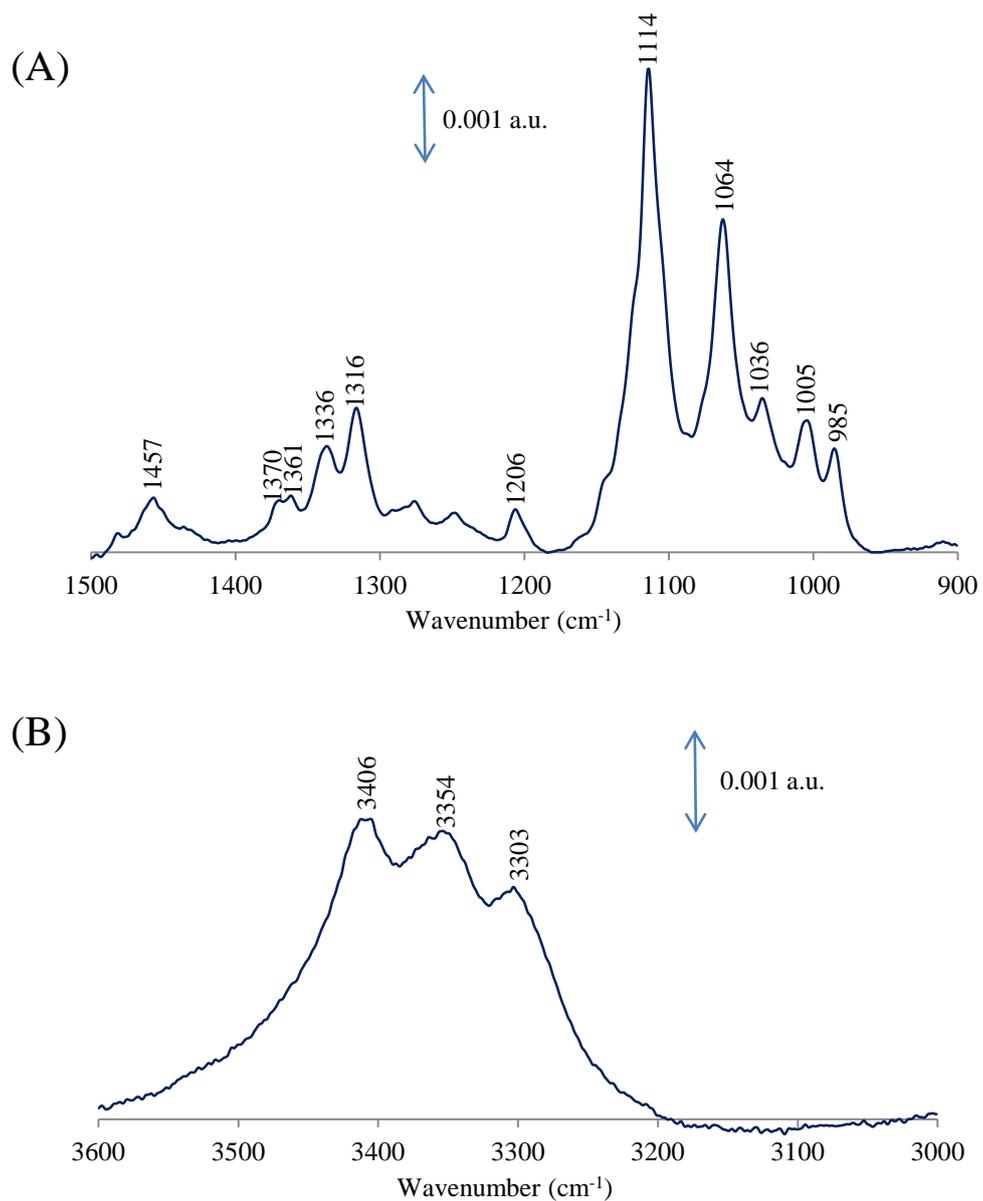
Figure 2.01. IRRAS spectrum of CNC films adsorbed to MUAM monolayer on evaporated gold substrate. Bands shown in (A) are characteristic of C–O stretching modes and of O–H bending modes for C–O–H alcohol groups. Bands shown in (B) are O–H stretching modes in C–O–H alcohol groups.

Table 2.1. Wavenumber assignments for peaks observed in IRRAS of cotton CNCs.

Wavenumber (cm^{-1})	Assignment[23]
985	Possibly C–O stretching in C6O6H primary alcohols
1005	C–O stretching in C6O6H primary alcohols
1036	C–O stretching in C6O6H primary alcohols
1064	C–O stretching in C2O2H secondary alcohol
1114	C–O stretching of a secondary alcohol C3O3H
1206	Symmetric C–O–C stretch of glycosidic links in C1O5C5 and C1O4C4
1316	O–H in plane bending in C–O–H groups
1336	O–H in plane bending in C–O–H groups
1361	O–H in plane bending in C–O–H groups
1370	O–H in plane bending in C–O–H groups
1457	O–H in plane bending in C–O–H groups
3303	O–H stretching in C6O6H primary alcohols
3354	O–H stretching of a secondary alcohol C3O3H
3406	O–H stretching in C6O6H primary alcohols
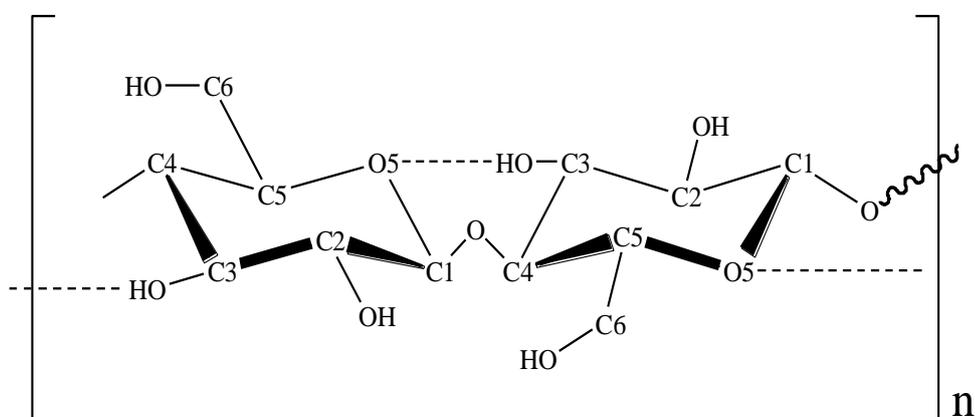
Figure 2.02. Schematic of single cellulose chain repeating unit of CNC.

2.3.1.2 AFM Images of CNC Films

Topographic AFM studies of CNC films on MUAM SAM on gold substrates were performed to better understand the CNC film morphology. Figure 2.03 A shows the topography image of MUAM monolayer on a thermal evaporated gold substrate. The gold film deposited by thermal evaporation process is characterized by a dense array of Au crystallites at room temperature.[27] The RMS roughness of the gold surface is approximately 3.8 nm. The thiol molecules are only approximately 1.5 nm in length and cannot be observed on the gold surface at this length scale.

The AFM height image of CNC film obtained from immersion in CNC solution on MUAM monolayer on gold is shown in Figure 2.03 B. As noted from the image, CNCs are rod-like particles, which is in agreement with previous results.[4] The RMS roughness of the CNC film on evaporated gold is about 4.5 nm as shown in the section graph in Figure 2.03 B. This AFM image displays a relatively uniform and densely packed CNC film, which can be used for further experiments as a substrate to investigate the interactions of proteins with CNCs.
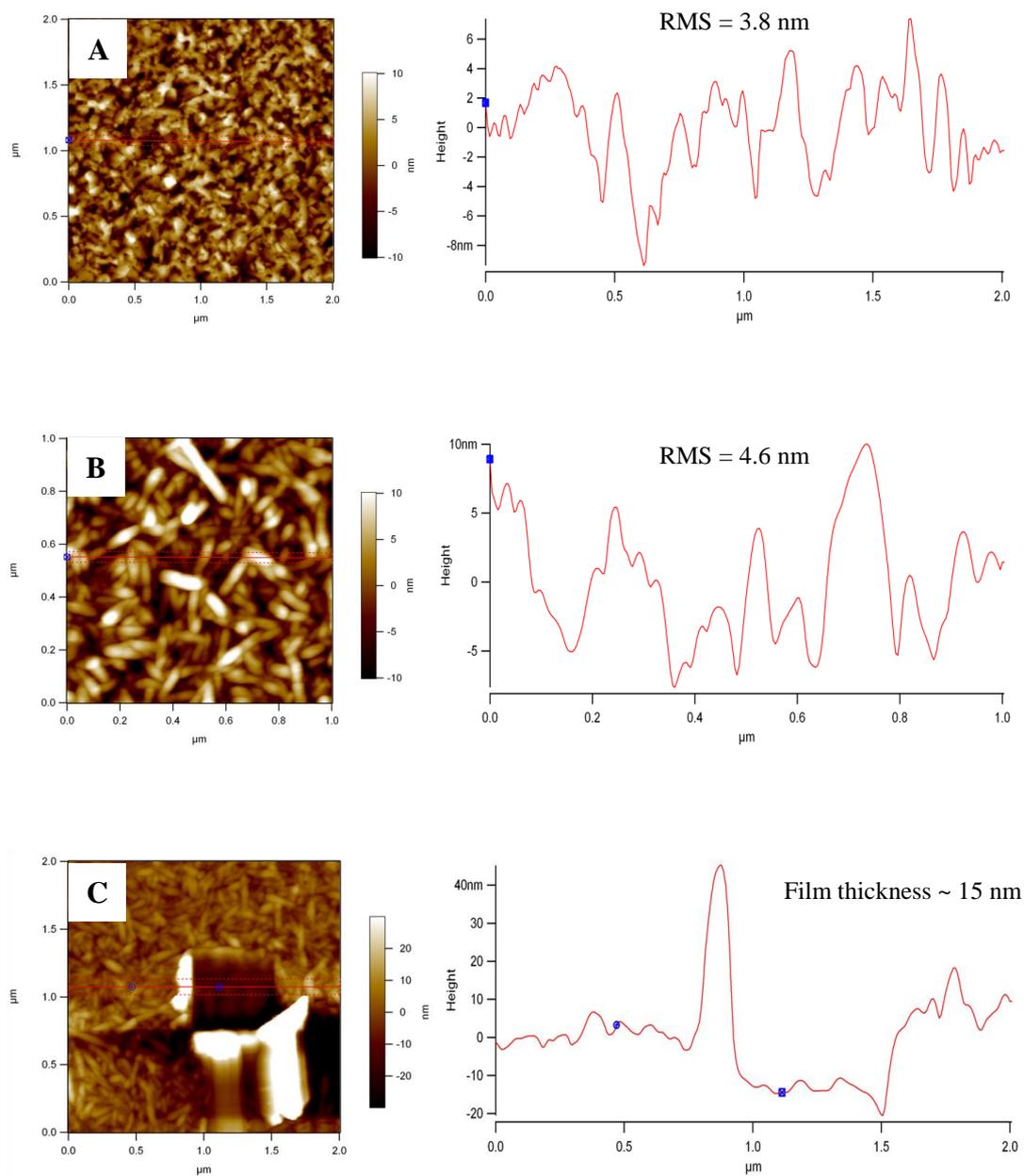
Figure 2.03. AFM images (AC mode, air) of (A) MUAM monolayer on evaporated gold substrate and (B) CNC films on substrate (A). The RMS values for MUAM layer on gold and CNC films are 3.8 nm and 4.6 nm, respectively. (C): CNC film thickness measurement by scratching the film. The thickness is approximately 15 nm.

To measure the thickness of the CNC film, an AFM scratching technique was utilized under contact mode (Figure 2.03 C). The length/width of nanostructures measured by an AFM typically contains tip effects and tip dilation errors. However, a height measurement, which is the CNC thickness measurement used in this study, is very accurate.[28] The thickness of the CNC film is approximately 15 nm. Knowing that the diameter of a CNC nanoparticle is 3–5 nm, this result indicates that a multilayered CNC film has been formed on MUAM modified gold substrate by immersion in the CNC solution.

2.3.2 Interactions between Proteins and Adsorbed CNC Films

2.3.2.1 IRRAS Studies and Protein Adsorption Isotherms

IRRAS is employed to assess the relative amount of bovine fibrinogen (BFG), bovine serum albumin (BSA) and chicken lysozyme (LYZ) adsorbed on MUAM monolayer with and without a CNC film. The MUAM monolayer substrate is used as a control. IRRAS spectra for BFG adsorption on both surfaces is shown in Figure 2.04 as an example. The region between 1500 and 1800 cm^{-1} contains characteristic bands of proteins and peptides. The amide I band (C=O stretch) is located in the region from 1650 to 1680 cm^{-1} and the amide II band (combination of C–N stretch and N–H bend) is observed near of 1550 cm^{-1}. These bands typically exhibit high intensity and are useful as a diagnostic indicator for adsorbed proteins.[29, 30] The absorbance of both the amide I and amide II bands have been used as a semi-quantitative measure of

the amount of protein adsorbed.[29-31] We used the amide I band absorbance in

the discussions below.
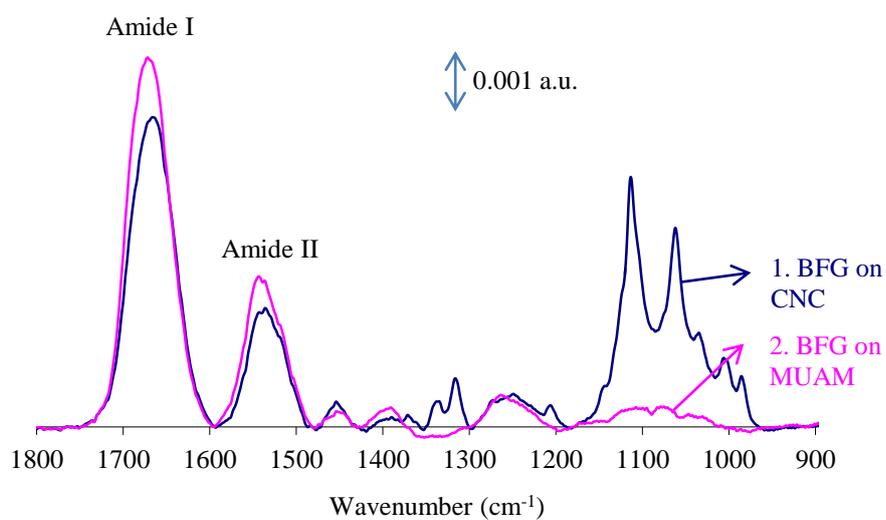
Figure 2.04. IRRAS spectra of BFG adsorption on CNC film surface (spectrum 1)

and on MUAM monolayer (spectrum 2) after exposure to 100 μg/ml BFG solution in PB

for 1 h.

IRRAS is also employed to develop protein adsorption isotherms. The MUAM monolayer substrates without CNC films are used as control, so protein adsorption behaviors on both CNC and MUAM surfaces are studied. Six concentrations are used in the experiment, so six IRRAS spectra have been obtained for each protein. The isotherms are plotted by the absorbance of amide I band against protein solution concentrations, and fitted to Langmuir isotherms using equation 2.1. The Langmuir model assumes monolayer coverage, where all adsorption sites are equivalent and adsorbing molecules do not interact with each other. The isotherms for BFG, BSA and LYZ adsorption on CNC and MUAM films are shown in Figure 2.05 A, B and C, respectively.

$$A = \frac{A_{max} K_{ads}[C]}{1 + K_{ads}[C]} \tag{2.1}$$

In equation 2.1, A refers to the amide I band absorbance, A_{max} is an asymptotic saturation value, [C] is the concentration of protein in solution, and K_{ads} is the adsorption constant. K_{ads} characterizes of the adsorption strength. All the fitting parameters using a one site Langmuir model are listed in Table 2.2. These parameters quantify the saturation amount of protein bound to the surface (A_{max}) and the strength of the interaction (K_{ads}) on CNC and MUAM surfaces.

In Figure 2.05, the amide I band absorbance increases with the protein concentrations until reaching a plateau. The maximum BFG adsorption on CNC films is slightly lower than that on MUAM monolayer which can partly be attributed to the electrostatic repulsion between the negatively charged BFG (iso-electric point=5.8) and negative CNC films. In spite of this, the maximum BFG adsorption is still higher than BSA or LYZ on the CNC films, which can be explained from the perspective of heterogeneous charge distribution over the fibrinogen molecule.[32, 33] Among the four domains of fibrinogen, D and E domains are negatively charged, but the αC domain bears net positive charges. Due to its large size and heterogeneous charge distribution, fibrinogen is very surface active and is capable of adsorbing to various materials. Therefore, though the overall charge of the fibrinogen molecules is negative, there are also regions on the fibrinogen molecule that are positively charged, which allows fibrinogen to have a fairly strong interaction with negatively charged CNC surfaces. In addition, multiple domains also make BFG capable of many types of interactions, such as van der Waals forces, H-bonding and dipole-dipole interactions. Similar results of fibrinogen deposition on negatively charged substrates under physiological conditions were previously reported.[34-39]

(A)
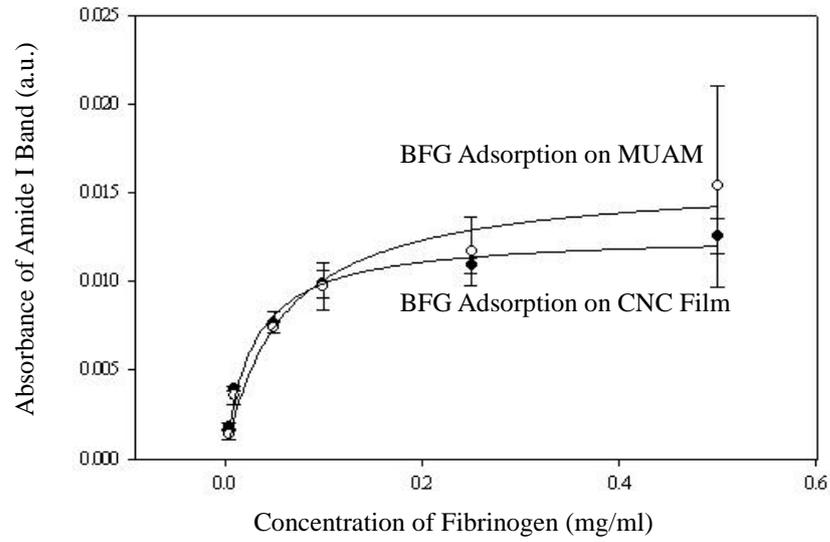
(B)
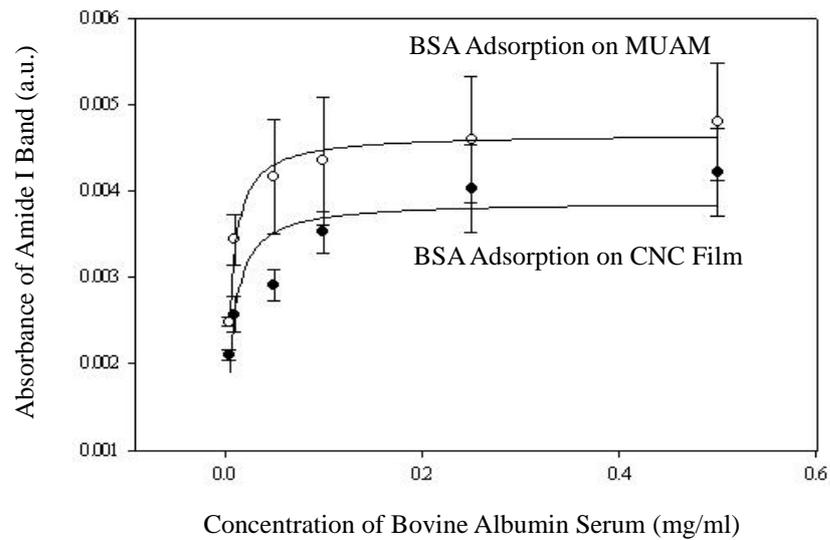
Figure 2.05. Isotherms of (A) BFG and (B) BSA adsorption on CNC films (filled circles) and MUAM monolayer (open circles). The points are the data and the curve is the one-site Langmuir fit.

(C)
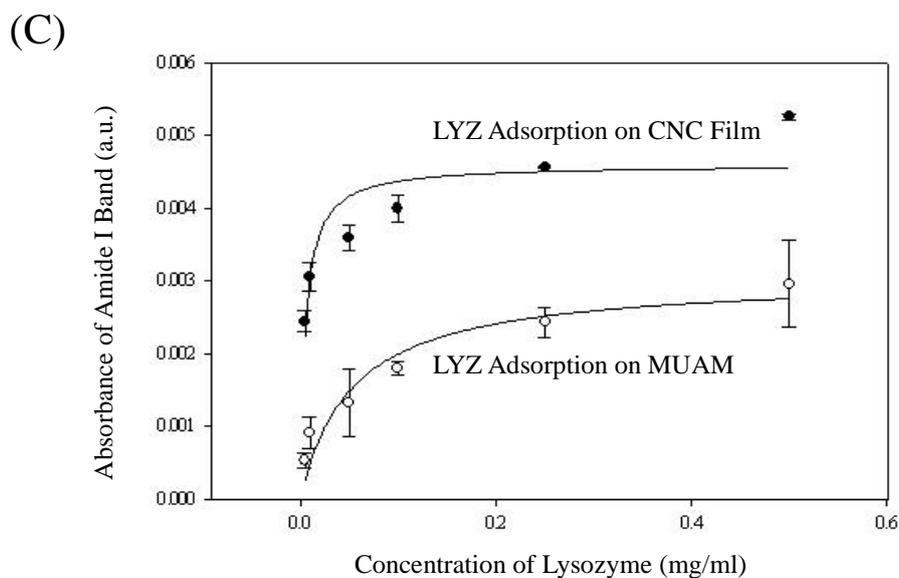
Figure 2.05. Continued.   Isotherm of (C) LYZ adsorption on CNC films (filled

circles) and MUAM monolayer (open circles). The points are the data and the curve is the

one-site Langmuir fit.

Table 2.2. Curve fitting parameters using a one-site Langmuir model for protein

(BFG, BSA and LYZ) adsorption isotherms obtained by IRRAS on CNC and MUAM

surfaces.

BFG Adsorption	R^2	A_{max} (a.u.)	K_{ads} (M^{-1})
CNCs	0.987	0.0127 ± 0.0005	$1.2\ (\pm 0.2) \times 10^7$
MUAM	0.967	0.016 ± 0.001	$6\ (\pm 2) \times 10^6$
BSA Adsorption	R^2	A_{max} (a.u.)	K_{ads} (M^{-1})
CNCs	0.824	0.0039 ± 0.0002	$1.3\ (\pm 0.4) \times 10^7$
MUAM	0.975	0.00470 ± 0.00009	$1.6\ (\pm 0.2) \times 10^7$
LYZ Adsorption	R^2	A_{max} (a.u.)	K_{ads} (M^{-1})
CNCs	0.803	0.0046 ± 0.0003	$3\ (\pm 1) \times 10^6$
MUAM	0.915	0.0030 ± 0.0004	$3\ (\pm 1) \times 10^5$

The A_{max} of BSA on CNCs is lower than that on MUAM, whilst the A_{max} of LYZ on CNCs is higher than that on MUAM, which can both be explained from the perspective of electrostatic forces. BSA (iso-electric point=4.7) is overall negatively charged under physiology conditions, so the repulsive forces between BSA and the negative CNC film make BSA molecules less favorable to adsorb on CNC films. On the contrary, LYZ (iso-electric point=11.0) is a cationic protein at pH 7.4. The negative charged groups on CNC surface make it attractive to LYZ proteins. It is difficult to compare the A_{max} values between different proteins due to the differences in molar weight (MW). For example, BFG (MW=340 kDa) will contain many more peptide bonds than LYZ (MW=14.5 kDa).

The K_{ads} values in Table 2.2. are dependent more on the protein than the surface. BFG (MW=340 kDa) and BSA (MW=66 kDa) are relatively large proteins that can interact with surfaces in a number of different ways (electrostatic interactions, hygrogen bonding, dipole-dipole interactions, etc.). LYZ (MW=14.5 kDa) is a much smaller and structurally stable "hard" protein. Hard proteins adsorb on hydrophilic surfaces only in cases in which the electrostatic interaction is favorable and strong enough and generally interacts more weakly with surfaces. [40, 41]
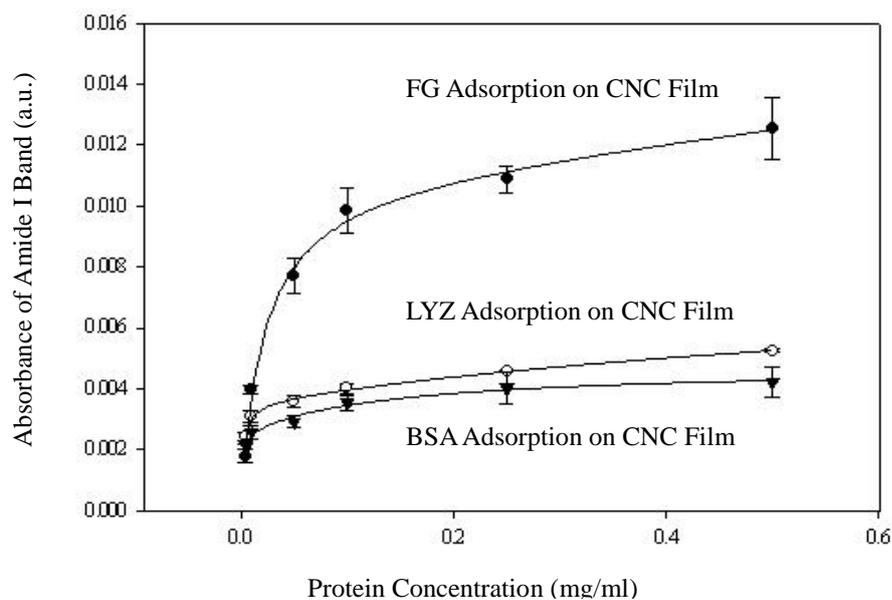
Figure 2.06. Isotherms of BFG (filled circles), BSA (filled triangles) and LYZ (open circles) adsorption on CNC film surface. The points are the data and the curve is fitted with the two-site Langmuir model.

Table 2.3. Curve fitting parameters using a two-site Langmuir model for protein (BFG, BSA and LYZ) adsorption isotherms obtained by IRRAS on CNC surfaces.

BFG	R^2	A_{max1} (a.u.)	K_{ads1} (M^{-1})	A_{max2} (a.u.)	K_{ads2} (M^{-1})
	0.994	0.011 ± 0.002	$1.7\,(\pm0.1)\times10^7$	/	/
BSA	R^2	A_{max1} (a.u.)	K_{ads1} (M^{-1})	A_{max2} (a.u.)	K_{ads2} (M^{-1})
	0.982	0.0025 ± 0.0007	$6.6\,(\pm0.8)\times10^7$	0.0022 ± 0.0005	$5.1\,(\pm0.6)\times10^5$
LYZ	R^2	A_{max1} (a.u.)	K_{ads1} (M^{-1})	A_{max2} (a.u.)	K_{ads2} (M^{-1})
	0.997	0.0036 ± 0.0002	$6.6\,(\pm0.4)\times10^6$	0.005 ± 0.004	$9.8\,(\pm0.6)\times10^3$

Considering the R^2 values in Table 2.2, it is apparent that the isotherms of

BSA and LYZ adsorption on CNC films are not well fitted using the Langmuir

model, which assumes one-site saturation ligand binding. It is possible that

there are exposed regions of the MUAM monolayer in the CNC films. This

would provide two sites for protein adsorption. So a two-site Langmuir model

was used to fit the isotherms of protein adsorption on CNC films using the

equation 2.2. The fitted isotherms are shown in Figure 2.06, and all the fitting

parameters are listed in Table 2.3.

$$A = \frac{A_{\max 1}K_{ads1}[C]}{1+K_{ads2}[C]} + \frac{A_{\max 2}K_{ads2}[C]}{1+K_{ads2}[C]} \tag{2.2}$$

Because we are fitting 6 data points with a 4 parameter fit, the standard

error due to the fit is relatively large for the K_{ads} values. The values for

uncertainties reported here are based on the run to run uncertainty.

Nevertheless, the improved R^2 values suggest that the two-site Langmuir is a

better fitting model. This observation indicates that the MUAM modified gold

substrate is not completely covered by CNC nanoparticles through

spontaneous adsorption. The exposed ammonium/amine groups also

contribute to the interactions with proteins. To prove this speculation, a thick

spin-coated CNC film is developed and will be discussed in later sections.

2.3.2.2 Protein Adsorption as a Function of CNC Coverage

The effect of CNC coverage was examined to assess the contribution of the underlying MUAM layer in the adsorption measurements. Drawn from previous work in our group, the CNC film thickness is highly dependent on the CNC suspension concentration and the incubation time. [42] A series of CNC films were prepared by immersion in different concentrations of CNC solutions for various time periods to attain different CNC coverage. Since the amount of CNC adsorbed onto MUAM layer is directly related to the C–O stretching band intensity, the coverage can be semi-quantitatively expressed by the intensity of the C–O band using IRRAS. 100 μg/ml proteins in PB were used to interact with CNCs on these prepared slides. The IRRAS spectra are shown in part A of Figures 2.07–2.09. The amounts of protein adsorption as a function of CNC coverage are plotted in part B of Figures 2.07–2.09.

Figure 2.07 A presents the IRRAS spectra of BFG adsorption on a series of CNC surfaces with different coverage. Figure 2.07 B demonstrates that the amide I peak intensity of fibrinogen decreases gradually with the increase of C–O stretching band intensity, which is likely due to the electrostatic repulsion between the negative CNC film and negatively charged BFG. However, the amide I peak is still quite intense even though the surface is mostly covered by CNCs. This observation indicates that fibrinogen has a very strong interaction with a complete CNC film, a MUAM SAM or a mixture of both, which is probably due to its active surface, large size and the ability to engage in other

interactions in addition to electrostatic forces with CNC films.
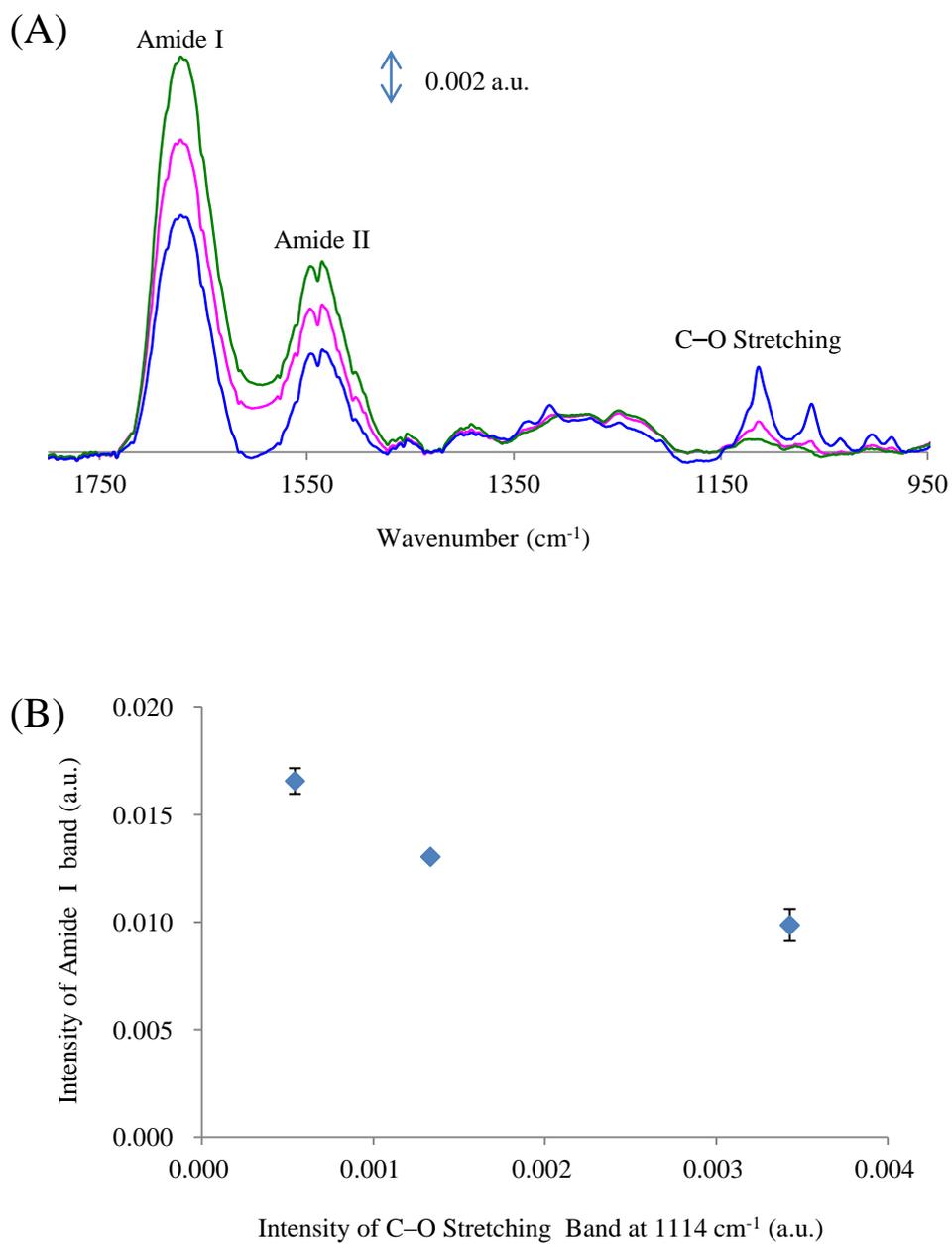
Figure 2.07. (A) IRRAS spectra of BFG adsorption on CNC films with different

CNC coverage. (B) Plot of BFG absorbance as a function of CNC coverage.

The relationship between BSA adsorption and CNC coverage is shown in Figure 2.08. Figure 2.08 A corresponds to the IRRAS spectra of BSA adsorption on a series of CNC surfaces with different CNC coverage. The plot of BSA adsorption vs. the CNC coverage is displayed in Figure 2.08 B. The BSA adsorption decreases with increasing amount of CNCs on the substrate. This is likely due to the electrostatic repulsion between the negative CNC film and the negatively charged BSA. To some extent, the thicker the CNC film is, the stronger the electrostatic repulsion. In addition, any exposed MUAM will be gradually covered by the increased amount of CNCs, which provides less chance for BSA to penetrate into CNC layers and interact with amine/ammonium groups. However, we speculate that the exposed MUAM cannot be completely covered by a 15 nm thick CNC film, so part of amide I peak intensity of BSA adsorption is attributed by the interaction between BSA and MUAM monolayer.

The spectroscopic results describing the interaction between LYZ and CNC surfaces with different coverage are contained in Figure 2.09 A. The absorbance of LYZ as a function of CNC coverage is plotted in Figure 2.09 B, which shows the LYZ absorbance intensifies as the CNC coverage increases. The observation can be explained from the perspective of electrostatic driven interactions we proposed.
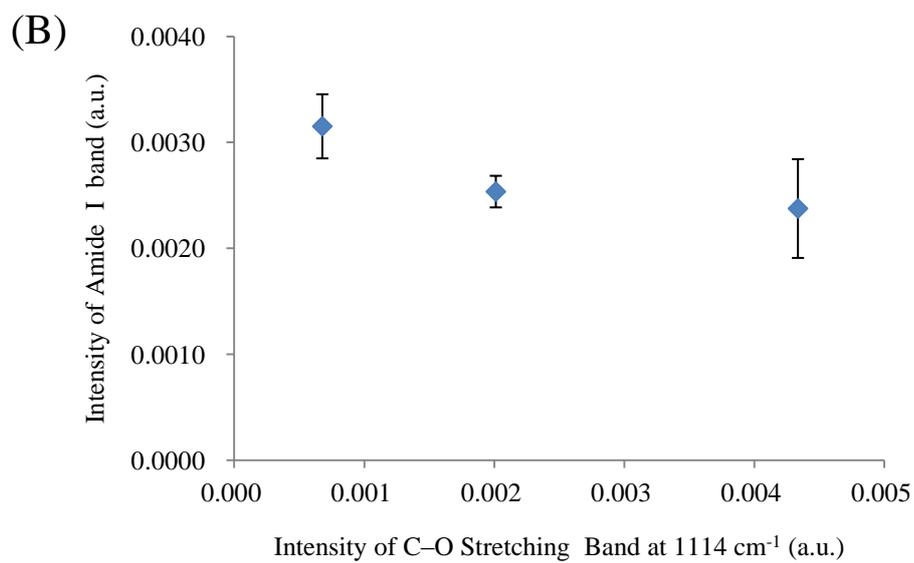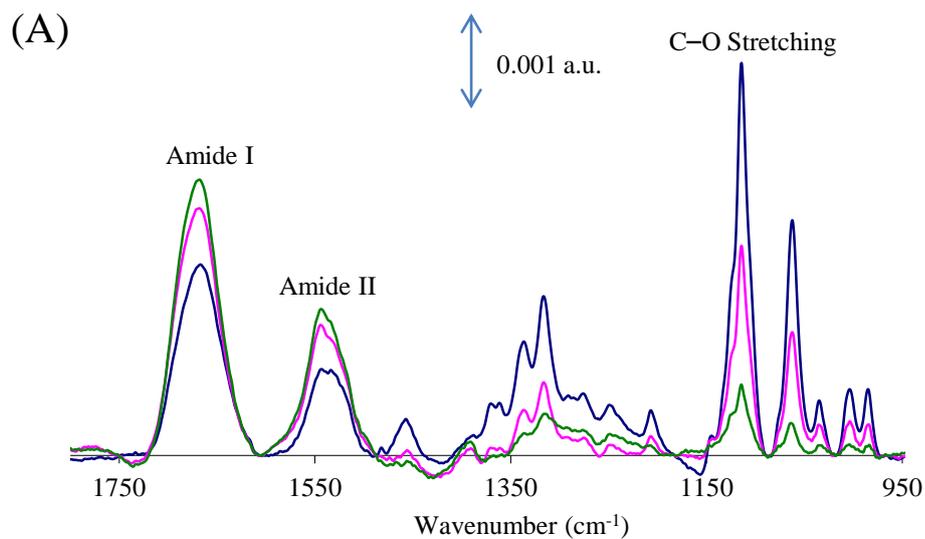
Figure 2.08. (A) IRRAS spectra of BSA adsorption on CNC films with different

CNC coverage. (B) Plot of BSA absorbance as a function of CNC coverage.
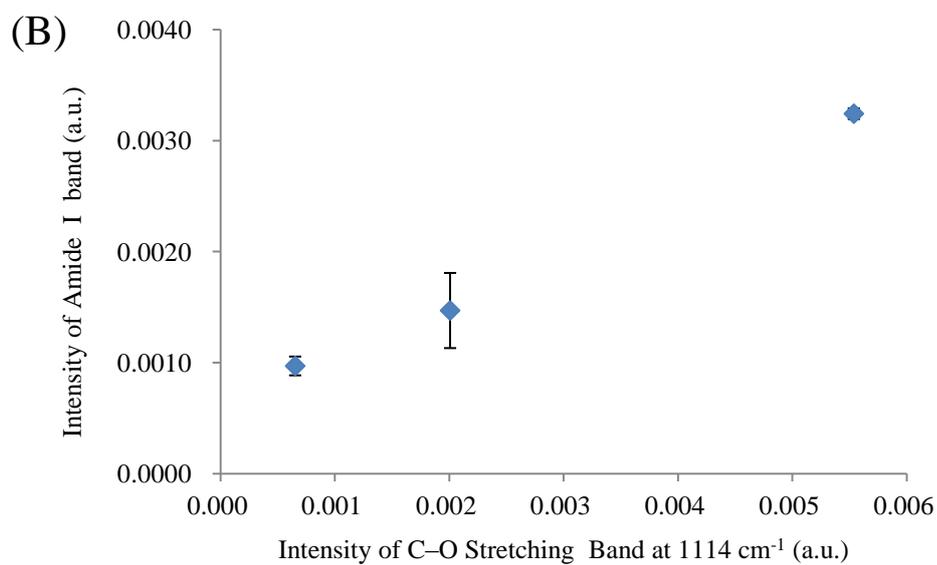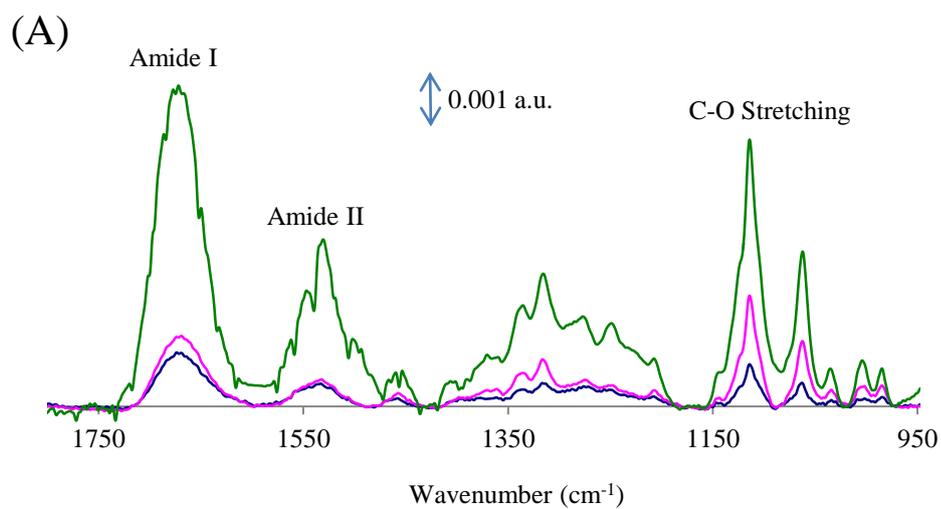
Figure 2.09. (A) IRRAS spectra of LYZ adsorption on CNC films with different

CNC coverage. (B) Plot of LYZ absorbance as a function of CNC coverage.

The results in Figure 2.07, 2.08 and 2.09 are in strong support of the speculation that electrostatic forces are responsible for the interactions between proteins and CNCs. The interactions may also depend on the intrinsic properties of proteins, such as charge distribution and protein size as is observed for BFG.

2.3.3 Spin Coated CNC Films

The experiments described above show that CNC films formed from spontaneous adsorption may contain exposed MUAM sites. In an attempt to completely cover the MUAM monolayer, thicker CNC films were prepared by spin coating. A series of CNC suspensions (0.5 wt%, 1.0 wt% and 2.0 wt%, and 3 wt%) were made to investigate the influence of CNC solution concentrations on the film thickness. Heating the samples after spin coating at 120 °C for 1 h is a necessary step to prevent CNCs from redispersing upon immersion in aqueous media.[14] The CNC films produced by this technique were characterized by AFM and IRRAS.

The infrared spectra corresponding to spin-coated CNC films made from CNC suspensions with various concentrations are shown in Figure 2.10 A. The region between 900 and 1500 cm^{-1}, which contains most of characteristic peaks for CNCs, was selected for interpretation. As discussed in Section 2.3.1.1, bands located at 985, 1005, 1036, 1064, 1114 and 1206 cm^{-1} refer to C–O stretching, and those at 1316, 1336, 1361, 1370 and 1457 cm^{-1} can be assigned to the O–H in-plane bending. A comparison of a spin coated CNC

film prepared by 3% CNC suspensions and a CNC film formed from spontaneous adsorption is shown in Figure 2.10 B. It is apparent that all characteristic peak intensities of spin coated CNC films increase significantly, indicating that the film thickness produced by spin coating is much higher than that by immersion.

Comparing the four spectra in Figure 2.10, it is obvious that the absorbance for C–O stretching bands and O–H in-plane bending bands increase with the CNC suspension concentration. The intensity of the C–O stretching band is correlated to the amount of CNCs adsorbed on the substrate; this observation suggests that the thickness of CNC films is strongly dependent on the concentration of the CNC solution used for spin coating preparation.

AFM scratching was employed to gain direct insights into the thickness of the CNC films produced by spin coating. The thickness measurements of CNC films prepared by 1 wt%, 2 wt% and 3 wt% CNC suspensions are shown in Figure 2.11 A, B and C, respectively. The thickness in Figure 2.11 A is 25 ± 2 nm, in B is around 36 ± 2 nm, and the thickness in C is 49 ± 2 nm. The data is in agreement with the IRRAS result that the films are thicker for greater CNC suspension concentrations. We expect that these "thicker" CNC films effectively block ammonium/amine groups on the MUAM monolayer. Protein adsorption to these films is probed in the next section.
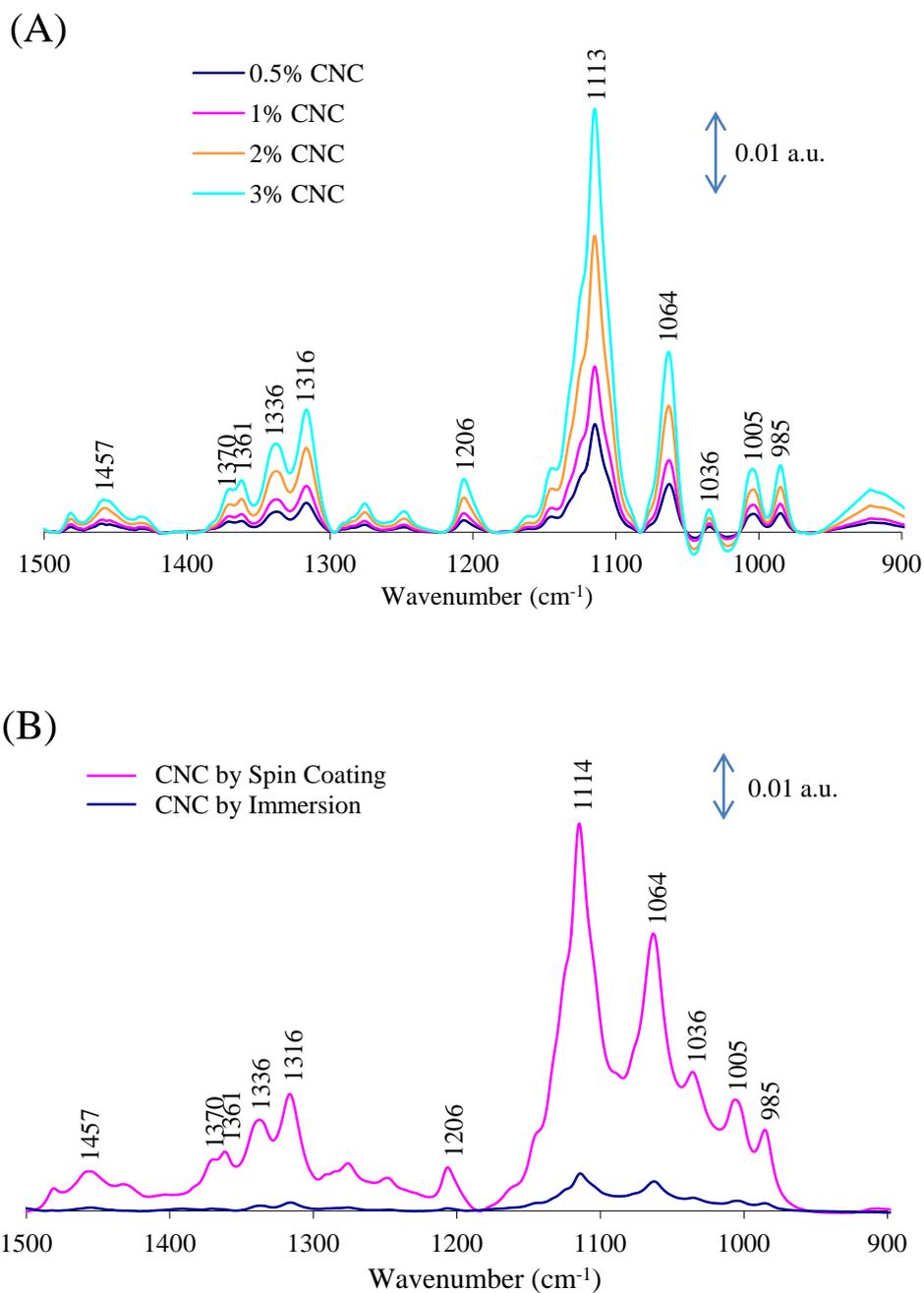
Figure 2.10. (A) IRRAS spectra of spin-coated CNC films prepared by CNC suspensions with different concentrations. (B) IRRAS spectra of (pink spectrum) spin-coated CNC films prepared by 3% CNC suspensions and (blue spectrum) of CNC films by spontaneous adsorption.
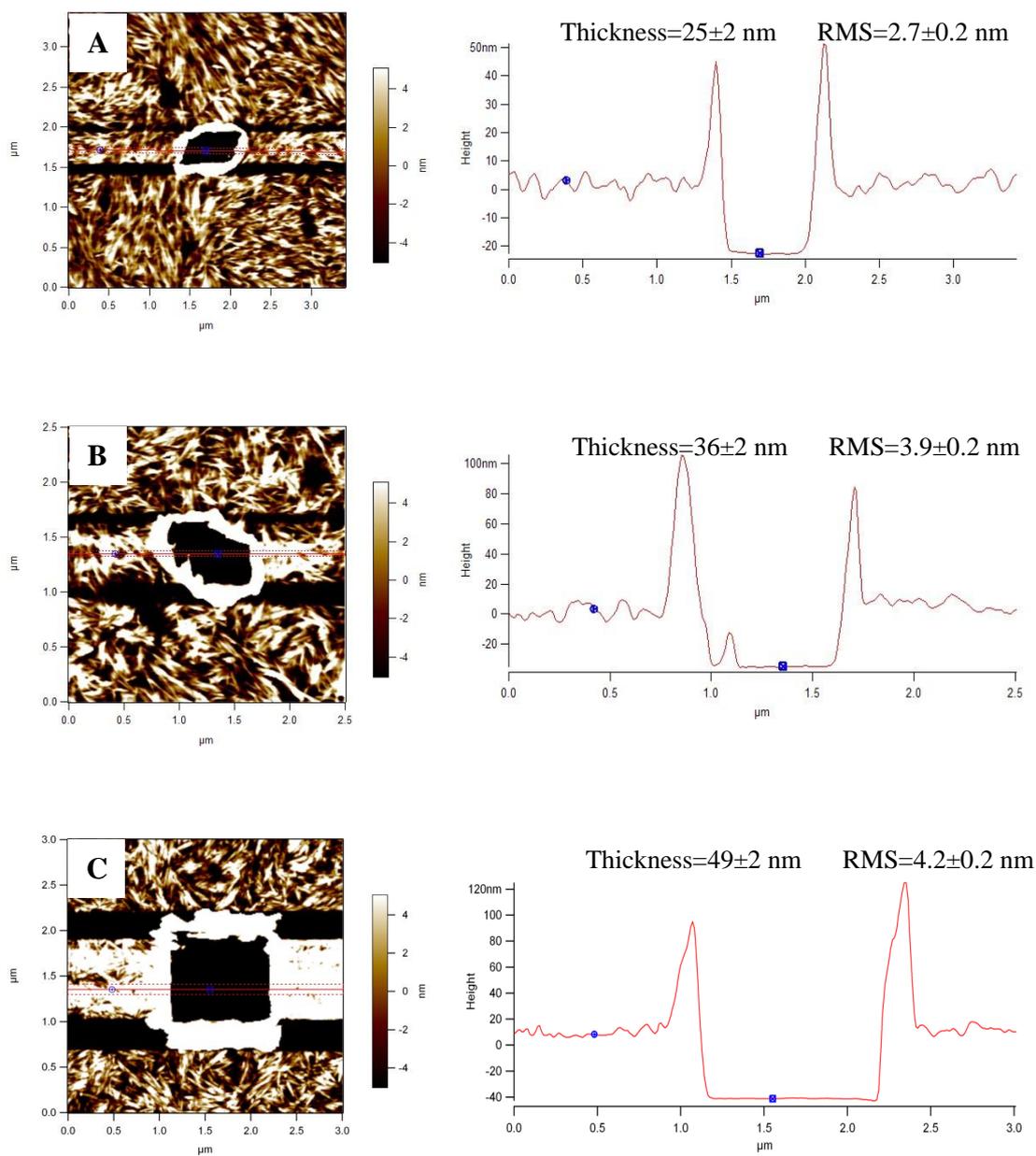
Figure 2.11. CNC film thickness measurements by scratching the film using AFM contact mode. (A) The thickness of spin coated CNC film made by 1 wt% CNC suspension is 25±2 nm. (B) The thickness of spin coated CNC film made by 2 wt% CNC suspension is 36±2 nm. (C) The thickness of spin coated CNC film made by 3 wt% CNC suspension is 49±2 nm.

2.3.4 Protein Adsorption on Thick CNC Films

We examined protein adsorption to the spin coated CNC film with the greatest thickness to ensure complete coverage of the MUAM monolayer. IRRAS was employed for assessing the relative amount of BFG, BSA and LYZ adsorbed on thick CNC films prepared by spin coating with 3 wt% CNC solutions. Infrared spectrum results are compared with the protein adsorption on CNC films prepared by immersion in 7.5×10^{-3} wt% CNC solution. IRRAS spectra of both surfaces after exposure to BFG, BSA and LYZ solution are shown in Figure 2.12 A, B and C, respectively.

Figure 2.12 A shows a much more intense amide I band for BFG adsorption to the thick, spin coated CNC film relative to the adsorbed CNC film. A comparison of the absorbance of the C–O stretch indicates that the spin coated CNC film (~0.06 a.u.) contains over 10× the amount of CNC particles as the adsorbed film (~0.004 a.u.). However, the difference in BFG adsorption is only a factor of 2. The higher adsorption of BFG on the thick, spin coated CNC film is not expected to be due to the lack of exposed ammonium/amine groups on the MUAM SAM. It has been shown that BFG adsorbs strongly to MUAM SAMs.[31] Our results below suggest that BFG adsorbs to CNC nanoparticles via a number of interactions (not only electrostatic forces). We believe that the thick CNC films contain a large surface area accessible to BFG. Our AFM results do not reveal a significant difference in roughness between adsorbed and spin coated CNC films. However, BFG molecules are

much smaller than the AFM tip size and may be able to access areas of the film that the tip cannot.

The adsorption of BSA on spin coated and immersed CNC films are shown in the spectra in Figure 2.12 B. It is interesting that the absorbance of BSA on spin coated film decreases approximately by a factor of ten compared to the absorbance on immersed CNC film. The result demonstrated that the thick spin coated CNC film effectively inhibits the non-specific adsorption of BSA. It provides strong evidence that electrostatic forces play a key role for BSA adsorption to CNC films. In addition, it was reported by Ying and coworkers that serum albumin preferentially adsorbs to hydrophobic surfaces.[43] Therefore, the BSA adsorption on hydrophilic CNCs is not a favorable process. Thicker CNC films reduce the likelihood of interactions between proteins and exposed ammonium/amine groups, and significantly inhibit the non-specific adsorption of negatively charged proteins such as BSA.
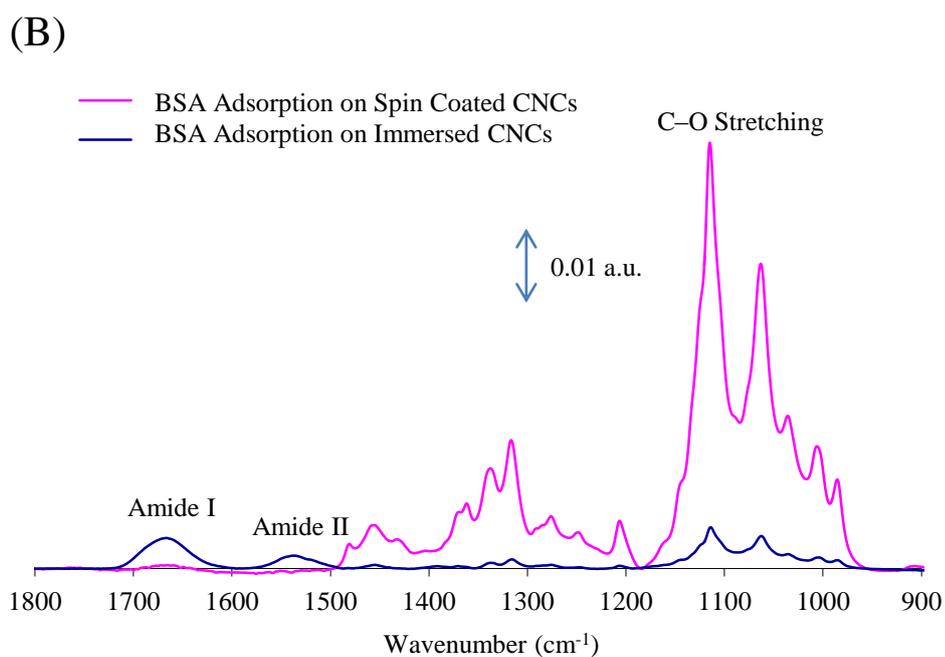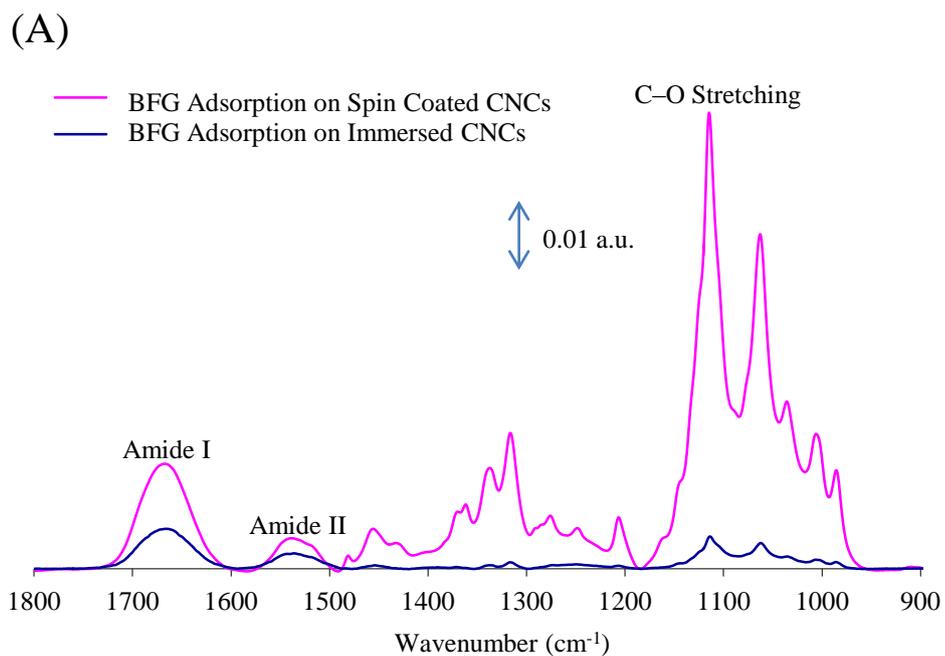
Figure 2.12. IRRAS spectra of (A) BFG and (B) BSA adsorption on spin coated CNC films prepared by 3 wt% CNC suspensions (blue spectrum) and on CNC films obtained by immersed in 7.5×10^{-3} wt% CNC solutions (pink spectrum).
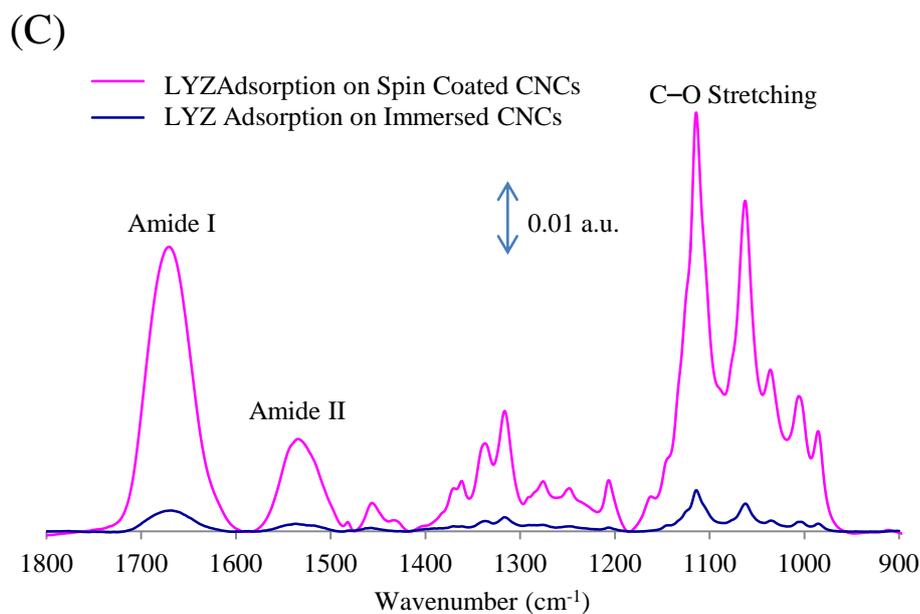
Figure 2.12. Continued. IRRAS spectra of (C) LYZ adsorption on spin coated CNC films prepared by 3 wt% CNC suspensions (blue spectrum) and on CNC films obtained by immersed in 7.5×10^{-3} wt% CNC solutions (pink spectrum).

The infrared spectra in Figure 2.12 C show LYZ adsorption on both spin coated and immersed CNC films. It is clear to see that LYZ adsorption increases significantly on spin coated CNC films. LYZ is a cationic protein at pH 7.4. The negative charged groups on CNC surface make it attractive to LYZ proteins. The thick CNC films completely block the exposed ammonium/amine groups, thus decreasing the repulsion between LYZ and the CNC surface. In addition, the surface area increases with the thickness of CNC films. Small sized LYZ molecules are able to penetrate into the CNC layers and interact with CNC particles in deep layers, which contribute to the

significant increase in the LYZ adsorption. This result provides more insight into the role of electrostatic forces in non-specific protein adsorption on CNC films.

Based on the IRRAS results, a comparison of the C–O stretching band intensity at 1114 cm^{-1} of CNC films prepared by both immersion and spin coating processes is shown in Figure 2.13 A and a comparison of amide I peak intensity after incubating the two CNC films to BFG, BSA and LYZ solutions is shown in Figure 2.13 B. It is apparent in part A that the absorbance of the C–O stretch for the spin coated CNC films (~0.06 a.u.) is greater than 10× the amount of CNC films obtained from immersion (~0.004 a.u.), which indicates greater thickness of spin coated CNC films. The similar absorbance of either surface also confirms the consistency of CNC preparation process through either spin coating or spontaneous adsorption.

Looking at the protein adsorption on the immersed CNC films, the amount of fibrinogen adsorbed is largest likely due to its active surface and multiple interactions with CNCs, while lysozyme adsorption is the least, which can be attributed to the repulsion from the exposed ammonium/amine groups. However on the spin coated CNC film which is thick enough to eliminate the contributions from ammonium/amine groups, the lysozyme adsorption becomes the largest and BSA adsorbs the least. This observation is in support of our hypothesis that electrostatic forces are mainly in responsible for the interaction between CNC films and proteins.
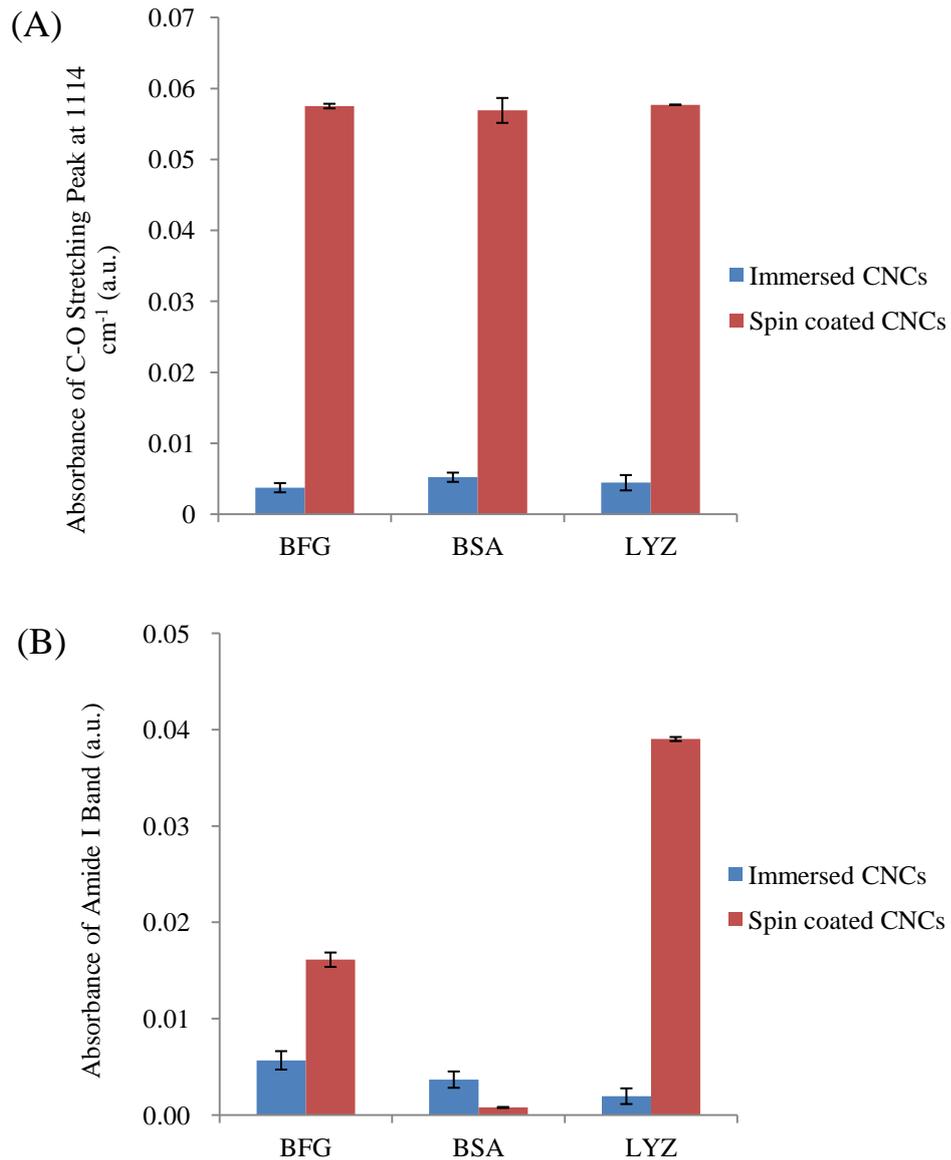
Figure 2.13. (A) Comparison of C–O stretching band intensity at 1114 cm^{-1} of CNC films prepared by (blue) immersion and (red) spin coating processes. (B) Comparison of amide I peak intensity of IRRAS spectra shown in Figure 2.11 after incubating CNC films prepared by (blue) immersion and (red) spin coating to BFG, BSA and LYZ solutions in phosphate buffer for 2 h.

2.3.5 Lysozyme Adsorption Isotherm on Thick CNC Films

To further prove that the contribution of exposed ammonium/amine groups to protein adsorption has been eliminated on thick CNC films, IRRAS is employed to develop protein adsorption isotherms. The isotherm for lysozyme is selected as an example because it has been shown that the exposed ammonium/amine groups have a significant influence to lysozyme adsorption on adsorbed CNC films according to the previous data. The isotherm is plotted by the absorbance of amide I band against the lysozyme solution concentrations, and fitted using a one site saturation ligand binding model with equation 2.1. All the fitting parameters are listed in Table 2.4 together with the parameters on spontaneous adsorbed CNC films for comparison.

The improved R^2 value demonstrates that the one site saturation ligand binding model fits the lysozyme isotherm on spin coated CNCs, and is consistent with the exposed ammonium/amine groups being covered by CNC particles. The maximum lysozyme coverage on spin-coated CNC films is almost 5× the amount on CNC films obtained from immersion. It is partly due to the screening of the charges between LYZ and any exposed ammonium/amine groups. In addition, the small sized LYZ molecules are likely to penetrate into CNC network and interact with CNC particles in deep layers, which also contribute the significant increase in the LYZ adsorption. The isotherm result is in strong support of our speculation that the contribution

of exposed ammonium/amine groups to protein adsorption has been eliminated

on thick CNC films and electrostatic forces play a key role in non-specific

protein adsorption on CNC films.
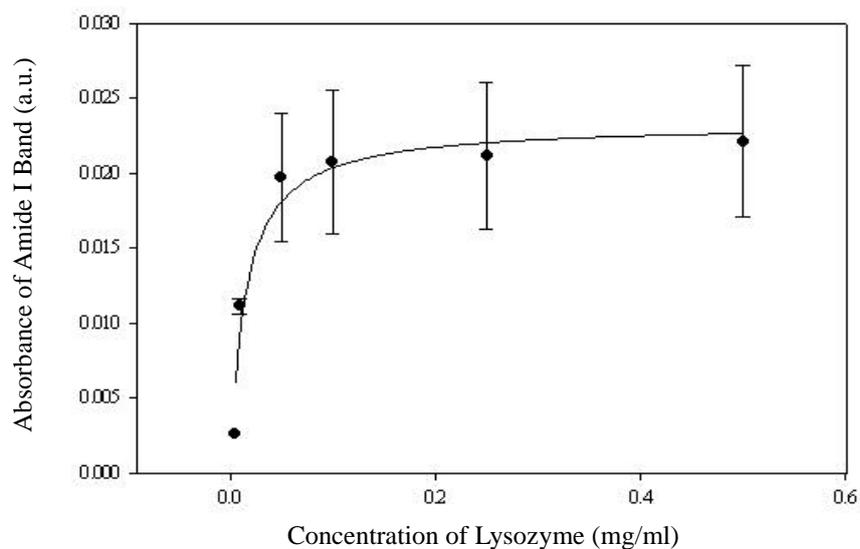
Figure 2.14. Isotherm of LYZ adsorption on spin-coated CNC films prepared by

1% CNC suspension . The points are the data and the curve is the one site saturation

fit.

Table 2.4. Curve fitting parameters using a one-site saturation model for LYZ

adsorption isotherm obtained by IRRAS on both spin-coated and spontaneous

adsorbed CNC surfaces.

LYZ Adsorption	R^2	A_{max} (a.u.)	K_{ads} (M^{-1})
Spin-coated CNCs	0.941	0.023±0.002	1.0 (±0.3) $\times 10^6$
Immersed CNCs	0.803	0.0046±0.0003	3 (±1) $\times 10^6$

2.3.6 Protein Adsorption on ε-Poly-L-lysine Modified CNC Surface

It is clear from the experiments described above that the negative charge on the CNC nanoparticles plays a large role in protein adsorption. In an effort to neutralize the negative charge we examined the adsorption of a cationic polymer. ε-Poly-L-lysine (ε-PLL) is a naturally occurring cationic polymer composed of L-lysine residues connected between ε-amino and α-carboxyl groups. ε-PLL dissolves in water producing a viscous liquid, which is biodegradable and non-toxic towards humans and the environment.[44] When PLL is applied to a surface, it renders the material with a larger number of positively charged sites available and increases the electrostatic attraction between the surface and the negatively charged molecules. In our experiment, spin coated CNC films were incubated in 1 % PLL solution for 30 min, and then used as protein adsorption substrates. IRRAS spectra of protein adsorption on the PLL modified CNC films are illustrated in Figure 2.15.

Figure 2.15 A shows fibrinogen adsorption on the PLL modified CNC film. The intensity of the amide I and amide II peaks demonstrate the strong interaction between fibrinogen and the PLL modified CNC surface. Compared with the result from BFG adsorption on unmodified CNC films, fibrinogen shows stronger attraction to PLL modified CNC surface.
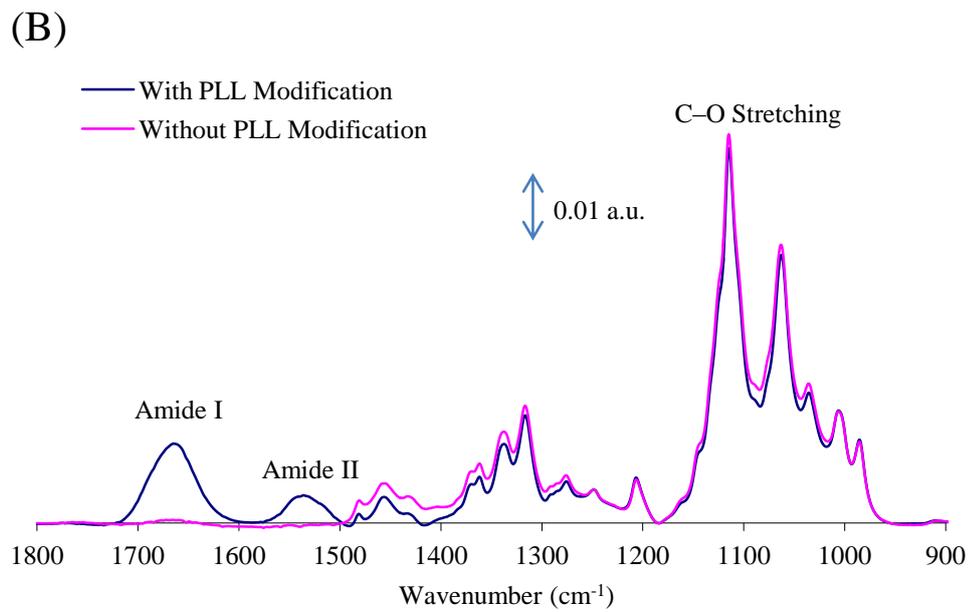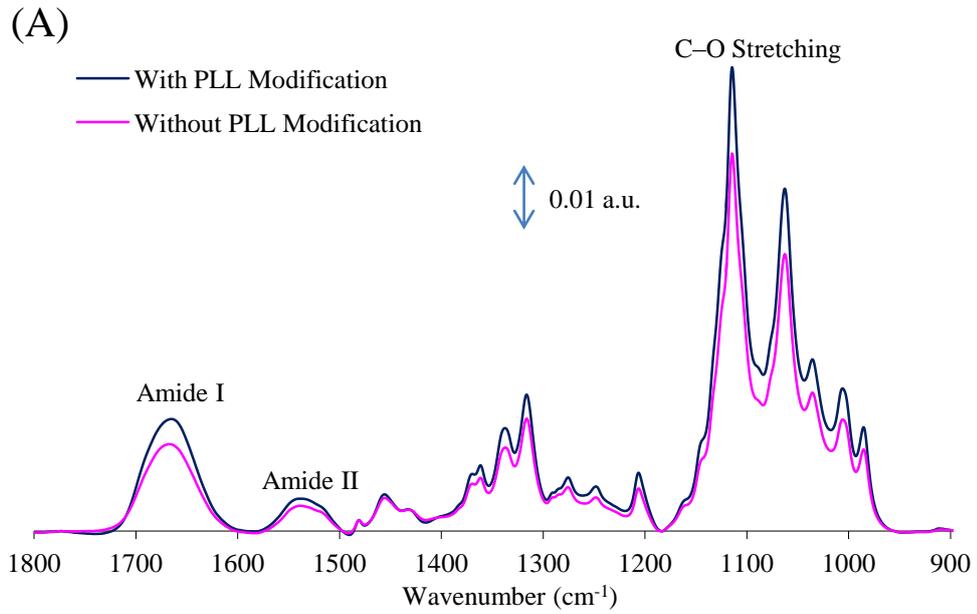
Figure 2.15. IRRAS spectra of (A) BFG and (B) BSA adsorption on spin coated

CNC films prepared by 3 wt% CNC suspensions (pink spectrum), and on PLL

modified CNC films spin coated by 3 wt% CNC suspensions (blue spectrum).

(C)
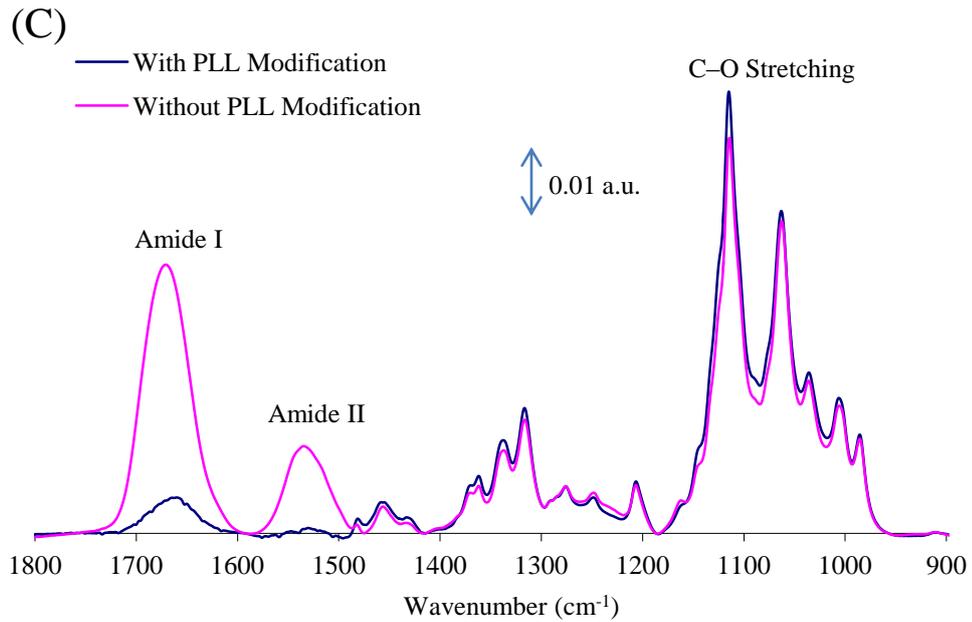
Figure 2.15. Continued. (C) IRRAS spectra of LYZ adsorption on spin coated CNC films prepared by 3 wt% CNC suspensions (pink spectrum), and on PLL modified CNC films spin coated by 3 wt% CNC suspensions (blue spectrum).

A similar increase of protein adsorption is observed for BSA as well which can be seen in Figure 2.15 B. After the CNC surface is coated by PLL, BSA adsorbs much more readily than on unmodified CNC films. The thick CNC film has the ability to inhibit non-specific adsorption of BSA, but loses this ability after immersion in PLL.

The PLL modified CNC surface exhibits lower attraction to lysozyme molecules as shown in Figure 2.15 C. In comparison with the spectrum of LYZ adsorption on unmodified CNC surface, the absorbance of the amide I and

amide II peaks decreases by a factor of six on the PLL modified surface, indicating the weaker interaction between lysozyme and PLL modified CNC film.

All of the results discussed above can be explained from the respect of electrostatic interactions. The initial CNC surface is negative due to the sulfate ester groups. The coating of PLL neutralizes part of the negative charges, and makes the surface positive. Due to the variations of the iso-electric points of the three proteins, LYZ is cationic while BSA and BFG are anionic under physiological conditions. Prior to the modification, CNC films preferably bind with positively charged proteins such as lysozyme, and limit the non-specific adsorption of negatively charged proteins such as BSA and BFG. After incubation in PLL solution, cationic PLL molecules cover the CNC film, and change the overall charge of the surface. As the surface becomes less negative, the interaction with positive proteins such as LYZ becomes small, but negative proteins (BFG and BSA) have stronger interactions with the lysine modified surface. All of the results in this experiment confirm that the electrostatic force is the major driving force responsible for the interactions between proteins and CNC films.

2.4 Conclusion

This chapter focused on the formation and characterization of CNC films, and investigated the interaction between CNC films and proteins. CNC films were formed via physisorption to an amine-terminated SAM on gold either by immersion in CNC suspensions or by a spin coating process. The thickness can be well controlled by CNC solution concentration. The thickness of spin coated CNC films is generally greater than CNC films prepared by immersion.

CNC films prepared by both approaches were used for investigating the interaction between CNCs and proteins. CNC films do not generally inhibit protein adsorption as we expected. The amount of protein adsorption depends on protein intrinsic properties such as molecular weight, charge distribution and iso-electric point. All the IRRAS and AFM imaging results reported in this chapter suggest that the major driving force responsible for the interaction between proteins and CNC films is electrostatic in nature. CNC films have a strong affinity for cationic proteins such as lysozyme, while exhibiting weak interactions with anionic proteins such as bovine serum albumin. Fibrinogen is an exception, due to its large size and heterogeneous charge distribution. Fibrinogen exhibits a strong interaction with CNC films due to its surface-active nature.

Due to the thin CNC films prepared by immersion, exposed ammonium/amine groups also contribute to non-specific protein adsorption through gaps in the CNC network. Yet the problem can be averted by using

thicker films prepared by spin coating. IRRAS results suggest that this thick CNC film prevent non-specific interactions with serum albumin, but has a significantly strong interaction with LYZ, which further provides proof that electrostatic forces play a key role in interactions between CNC film and proteins. Efforts to neutralize charges failed in that we went from a negative film to a positive one to some extent. However, optimization of PLL coating may be able to better balance the charge of CNC film.

2.5 References

1. Bai, W.; Holbery, J.; Li, K. C. *Cellulose* **2009**, *16*, 455–465.

2. Elazzouzi-Hafraoui, S.; Nishiyama, Y.; Putaux, J. L.; Heux,L.; Dubreuil, F.; Rochas, C. *Biomacromolecules,* **2008**, *9*, 57–65.

3. Samir, M. A. S. A.; Alloin, F.; Dufresne, A. *Biomacromolecules* **2005**, *6*, 612–626.

4. Lahiji, R. R.; Xu, X.; Reifenberger, R.; Raman, A.; Rudie, A.; Moon, R. J. *Langmuir* **2010**, *26*, 4480–4488.

5. Yang, H.; Tejado, A.; Alam, N.; Antal, M.; van de Ven, T. G. M. *Langmuir* **2012**, *28(20)*, 7834–42.

6. Sievens-Figueroa, L.; Bhakay, A.; Jerez-Rozo, J. I.; Pandya, N.; Romañach, R. J.; Michniak-Kohn, B.; Iqbal, Z.; Bilgili, E.; Davé, R. N. *International Journal of Pharmaceutics* **2012**, *423(2)*, 496–508.

7. Roland, J. C.; Mosiniak, M.; Roland, D. *Acta Botanica Gallica* **1995**, *142(5)*, 463–484.

8. Dash, R.; Ragauskas, A. J. *RSC Advances* **2012**, *2*, 3403-3409.

9. Li, F.; Biaginoni, P.; Finazzi, M.; Tavazzi, S.; Piergiovanni, L. *Carbohydrate Polymers* **2013**, *92(2)*, 2128−2134.

10. Choi, Y. J.; Simonsen, J. *Journal of Nanoscience and Nanotechnology* **2006**, *6(3)*, 633−639.

11. Zhao, Q.; Sun, G.; Yan, K.; Zhou, A.; Chen, Y. *Carbohydrate Polymers* **2013**, *91(1)*, 169−174.

12. Kontturi, E.; Johansson, L-S.; Kontturi, K. S.; Ahonen, P.; Thune, P. C.; Laine, J. Langmuir 2007, 23(19), 9674−9680.

13. Gunnars, S.; Wågberg, L.; Cohen Stuart, M.A. *Cellulose* **2002**, *9*, 239–249.

14. Edgar, C. D.; Gray, D. G. *Cellulose* **2003**, *10***,** 299–306.

15. Ahola, S.; Turon, X.; Osterberg, M.; Laine, J.; Rojas, O. J. *Langmuir* **2008**, *24 (20)*, 11592–11599.

16. Cranston, E. D.; Gray, D. G. *Science and Technology of Advanced Materials* **2006**, *7 (4)*, 319–321.

17. Wang, Y.; Zhang, L. *Journal of Nanoscience and Nanotechnology* **2008**, *8 (11)*, 5831−5838.

18. Martinez, A. W.; Phillips, S. T.; Whitesides, G. M. *Analytical Chemistry* **2010**, *82*, 3–10.

19. Su, S.; Ali, M. M.; Filipe, C. D. M.; Li, Y.; Pelton, R. *Biomacromolecules* **2008**, *9*, 935–941.

20. Tan, S. N.; Ge, L.; Tan, H. Y.; Loke, W. K.; Gao, J.; Wang, W. *Analytical Chemistry* **2012**, *84*, 10071–10076.

21. Martinez, A. W.; Phillips, S. T.; Butte, M. J.; Whitesides, G. M. *Angewandte Chemie International Edition* **2007**, *46*, 1–4.

22. Benmakroha, Y.; Zhang, S.; Rolfe, P. *Medical and Biological Engineering and Computing* **1995***, 33,* 811–821.

23. Walker, S.; Straw, H. *Spectroscopy*, Chapman and Hall, London, 1962.

24. Liang, C. Y.; Marchessault, R. H. *Journal of Polymer Science* **1959**, *39*, 269–278.

25. Blackwell, J.; Vasko, P. D.; Koenig, J. L. *Journal of Applied Physics* **1970**, *11*, 4375–4379.

26. Maréchal, Y.; Chanzy, H. *Journal of Molecular Structure* **2000**, *523*, 183–196.

27. Shewchuk, D. M.; McDermott, M. T. *Langmuir* **2009**, *25(8)*, 4556-63.

28. Araki, J.; Wada, M.; Kuga, S.; Okano, T. *Colloids and Surfaces A: Physicochemical and Engineering Aspects* **1998**, *142*, 75–82.

29. Lenk, T. J.; Horbett, T. A.; Ratner, B. D. *Langmuir* **1991**, *1991*, 1755–1764.

30. Liedberg, B.; Ivarsson, B.; Lundstrom, I. *Journal of Biochemical and Biophysical Methods* **1984**, *9*, 233–243.

31. Ta, T. C.; McDermott, M. T. *Analytical Chemistry* **2000**, *72*, 2627–2634.

32. Adamczyk, Z.; Bratek-Skicki, A.; Dabrowska, P.; Nattich-Rak, M. *Langmuir* **2012**, *28*, 474–485.

33. Wasilewska, M.; Adamczyk, Z. *Langmuir* **2011**, *27(2)*, 686–696.

34. Zembala, M.; Dejardin, P. *Colloids and Surfaces B* **1994**, *3*, 119–129.

35. Ortega-Vinuesa, J. L.; Tengvall, P.; Lundstrom, I. *Thin Solid Films* **1998**, *324*, 257–273.

36. Ortega-Vinuesa, J. L.; Tengvall, P.; Lundström, I. *Journal of Colloid and Interface Science* **1998**, *207*, 228–239.

37. Malmsten, M. *Journal of Colloid and Interface Science* **1994**, *166*, 333–342.

38. Kalasin, S.; Santore, M. M. *Colloids and Surfaces B* **2009**, *73*, 229–236.

39. Toscano, A.; Santore, M. M. *Langmuir* **2006**, *22*, 2588–2597.

40. Hayens. C. A.; Norde, W. *Journal of Colloid and Interface Science* **1994**, *169*, 313–328.

41. Nakanishi, K.; Sakiyama, T.; Imamura, K. *Journal of Bioscience and Bioengineering* **2001**, *91(3)*, 233–244.

42. Kaufman, G.; McDermott, T. M. manuscript in preparation.

43. Ying, P.; Yu, Y.; Jin, G.; Tao, Z. *Colloids and Surfaces B* **2003**, *32*, 1–10.

44. Shih, I. L.; Shen, M.H. *Mini Reviews in Medicinal Chemistry* **2004**, *4*, 179–188.

Chapter 3 Cellulose Nanocrystal (CNC) Films as a Platform for Immunoassays

3.1 Introduction

In the previous chapter, we examined interactions between proteins and CNC films. CNC films have the ability to inhibit non-specific adsorption of anionic proteins such as serum albumin and show a strong affinity to cationic proteins driven by electrostatic forces. Protein adsorption onto solid surfaces is also of significance in various applications. For example, a critical step in construction of any surface based immunoassay is the immobilization of receptor molecules onto a surface. Therefore understanding of protein adsorption onto solid surfaces is a key issue in the design of biosensors.

Maximizing the number of receptor molecules will result in a larger response when detecting the analyte of interest, as more target molecules could be captured per unit area.[1] A dense CNC film can potentially provide a high surface area substrate to which probe molecules (antigen or antibody) can be immobilized. The attachment for proteins can be either physically[2, 3] or chemically[4-6] mediated, with both having advantages. Typically hydrophobic or electrostatic interactions between the protein and the solid phase are involved in physical adsorption. It is generally an experimentally simple method and often retains the activity of the protein.[7] The disadvantage of physical adsorption is the instability. The adsorption process can be reversible

with protein being desorbed by certain buffers or detergents, or replaced by other proteins in solution.[8, 9] In contrast, chemical immobilization involves the formation of covalent bonds between the protein and the solid surface. This method is experimentally more difficult, but results in irreversible binding of protein to the surface, which makes this approach popular.[10-13]

For covalent immobilization of proteins, one of the most common procedures involves the formation of an amide bond between the protein and surface. One method for amide bond formation involves conversion of a carboxylic acid group of the solid surface to an N-hydroxysuccinimide (NHS) ester using 1-ethyl-3-(3-dimethylaminopropyl) carbodiimide (EDC).[14-16] Reaction of the primary amine in proteins from lysine residues or the N-terminus with the NHS ester via nucleophilic displacement results in the formation of an amide bond.[17] The structures of NHS and EDC are illustrated in Figure 3.01 A and B, and the mechanism of amide bond formation involving the terminal carboxylic acid group and NHS is shown in Figure 3.01 C.

Successful formation of the ester intermediate depends on the accessibility of the terminal carboxylic acid groups, which do not exist in CNC nanoparticles. So functionalization of the CNC surface with carboxylic acid terminal groups is a prerequisite first step. We utilize the phenylacetic acid diazonium salt (dPAA) to realize a CNC surface functionalization.

(A)

N-hydroxysuccinimide (NHS)

(B)

1-ethyl-3-(3-dimethylaminopropyl) carbodiimide

(C)
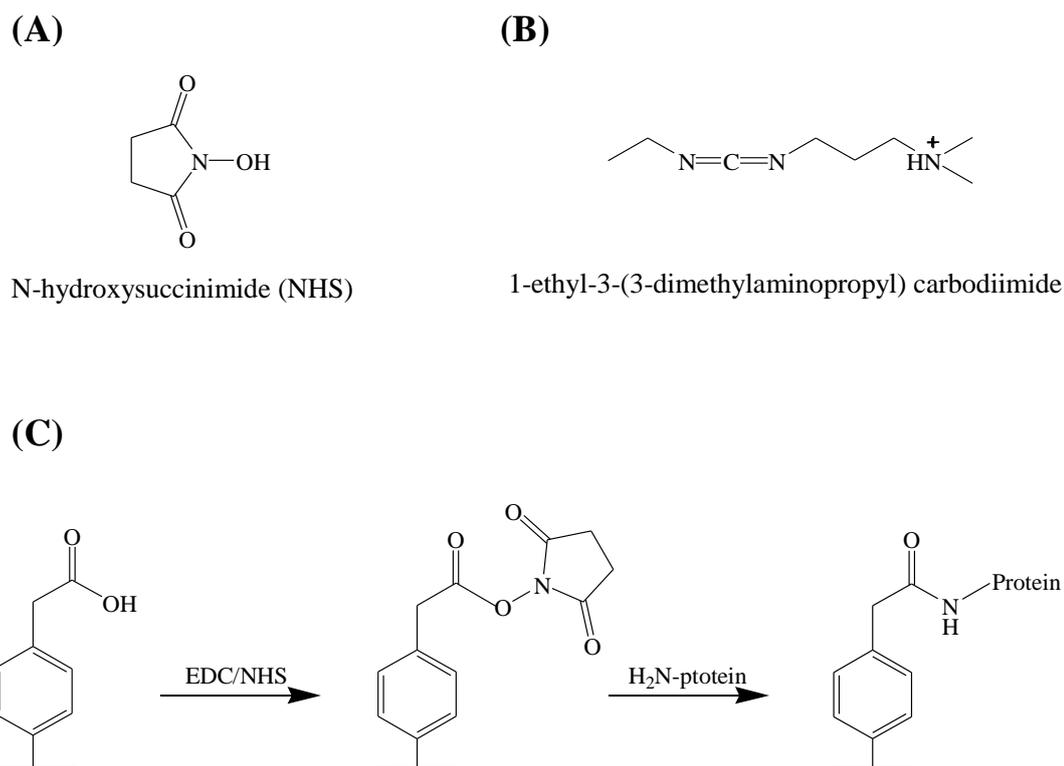
Figure 3.01. (A) Structure of N-hydroxysuccinimide (NHS). (B) Structure of 1-ethyl-3-(3-dimethylaminopropyl) carbodiimide (EDC). (C) The strategy for immobilizing protein onto the carboxylic acid-terminated phenylacetic acid diazonium salt.

Aryl diazonium salts were first used to modify carbon substrates by Pinson and coworkers in 1992.[18] This chemistry resulted in the formation of a covalent C-C bond on carbon substrates such as glassy carbon,[19, 20] highly ordered pyrolytic graphite (HOPG),[19, 21, 22] and pyrolyzed photoresist films (PPF)[23]. The accepted mechanism involves the reduction of the diazonium ion by an external potential and the formation of an aryl radical intermediate in close proximity to the conductive substrate.[24] This radical intermediate then binds to the surface to form the initial film. Further, excess aryl radical intermediates could attack already attached molecules on the surface to form multilayers.[25] However, steric packing of the multi-layer acid groups can limit the rate of NHS ester intermediate formation, which significantly decreases the efficiency of the reaction. In our studies electrochemistry is not applicable for the non-conductive CNC film, so we utilized a reducing agent L-ascorbic acid to provide diazonium salts with electrons to form the radical intermediates. This method was developed by Dr. Du in our group.[26] Phenylacetic acid diazonium salt which terminates with a carboxylic acid was selected to modify CNC surfaces. The proposed mechanism of the spontaneous reduction of phenylacetic acid diazonium cation at a CNC surface with the loss of molecular nitrogen is displayed in Figure 3.02. After the NHS activation process (Figure 3.01 C) antibodies are then chemically immobilized on the modified CNC surface. However, this supposition remains to be proven.

Figure 3.02. Assumed mechanism for the spontaneous reduction of phenylacetic

acid diazonium cation at a CNC surface resulting in a multilayered film.

Immunoassays employ antibodies to recognize and bind with an analyte. Antibodies are a class of proteins called immunoglobulins, which are major components of the immune system response to foreign substances (antigens). Antibodies can be mainly found in blood and extracellular fluid and control the infection of body tissues. There are several classes of immunoglobulins (IgA, IgD, IgE, IgG, and IgM) which are classified based on their functions. The binding is highly selective and this specificity is fundamental to immunoassays.[27] In our studies, IgG antibodies and their complementary antigens were utilized.

Surface plasmon resonance (SPR) is a label-free technique that can be used in the detection of antibody-antigen binding. Since the late 1990's, SPR biosensors have become a main tool for the study of biomolecular interactions both in life science and pharmaceutical research.[28, 29] The SPR method is based on optical measurement of refractive index changes associated with the binding of analyte molecules in a sample to biorecognize molecules immobilized on the SPR sensor. The observed SPR signal is related to the molecule's mass and the affinity of the interaction. Therefore, antibody-antigen binding results in the mass increase on the surface, thus increasing the SPR detection signal.

The goal of this chapter is to develop and evaluate the usefulness of a CNC surface as a substrate for immunoassays. A dense CNC film will provide a high-surface area substrate and the polysaccharide based structure of CNCs

can potentially resist non-specific adsorption of proteins. It has been reported in the literature that molecular layers of polysaccharides significantly inhibit the non-specific adsorption of proteins.[30] In this chapter, we will use infrared reflection absorption spectroscopy (IRRAS) to examine both physical and chemical processes to immobilize IgG antibodies on spin coated CNC films. Prior to the chemical immobilization process CNC films are pre-modified with phenylacetic acid diazonium salt (dPAA) to introduce carboxylic acid groups on the CNC surface. Surface plasmon resonance (SPR) will be employed to detect the antibody-antigen binding. The application of CNC films as a platform for biosensing will be of importance for developing biosensing platforms by utilizing the unique structure and property of CNC nanoparticles.

3.2 Experimental

3.2.1 Preparation of Gold Substrates

All glass substrates and glassware were cleaned with hot piranha solution (1:3 30% H_2O_2: 98% H_2SO_4) for 15 min followed by rinsing thoroughly with deionized (18.2 MΩ)/filtered water (NANOpure™ water purification system, Barnstead International, Dubuque, Iowa). Substrates were blown dry using argon gas. 99.99% Au shot (Goodfellow) was used to deposit gold for all substrates via thermal evaporation (Torr International, INC). For SPR chips, a 45 nm gold thick film was deposited on SF10 glass (Schott; Toronto, ON, Canada). 1 nm of chromium (ESPI Metals) was deposited in between the glass

slide and the gold film for better adhesion. For the IRRAS microscope slides, substrates consisted of 300 nm gold with a 15 nm adhesive layer of Cr.

3.2.2 Preparation of CNC Films

The gold substrates were first cleaned with UV/ozone treatment for 15 min, and then soaked in 100 μM mercaptoundecylamine hydrochloride (MUAM, HS−(CH$_2$)$_{11}$−NH$_2$·HCl) for 24 h, followed by a thorough rinse with anhydrous ethanol to remove unbound alkanethiolate from surface. Spin coating was used for making thick and smooth CNC films. A 1.0 wt% CNC water suspension was prepared by sonicating for 30 min, followed by filtered through a 0.45 μm membrane to get rid of large agglomerates. 500 μl CNC solutions were dropped from a micropipette onto MUAM self-assembled SPR chips and spun at 4000 RPM for 60 s using a PWM32 Series Photoresist Spinner (Headway Research. Inc., Garland, Texas, USA). A volume of 2 ml of CNC suspensions was used for coating the microscope slides. The samples were heated after spin coating at 120 °C for 1 h to prevent CNCs from redispersing when the slides were wetted.

3.2.3 Protein Physisorption on CNCs

Phosphate buffer (PB) was prepared by adding 0.1 M sodium hydroxide (NaOH, CALEDON Lab Ltd., Georgetown, ON, Canada) solution drop by drop to 1 mM reagent grade sodium phosphate, monobasic (NaH$_2$PO$_4$·H$_2$O, Sigma, St. Louis, MO, USA), meanwhile measuring the pH of the mixed solution using a pH meter (XL 50, Accumet, Fisher Scientific) until the pH

value reached 7.4. As the CNCs are sensitive to the ionic strength, the absence of chloride and potassium ions in this lab-made phosphate buffer prevents the aggregation of CNC when incubating the CNC in protein solutions. Immunoglobulin G (IgG) antibodies (MP Biomedicals, LLC, Solon, OH, USA) were prepared to concentrations of 100 μg/ml with phosphate buffer. IgG antibodies were adsorbed onto the CNC modified substrates by soaking the slides in protein solutions for 2 h for complete adsorption, followed by rinsing with 1 mM PB thoroughly and blow drying with argon.

3.2.4 Protein Chemisorption on Phenylacetic Acid Diazonium Salt Modified CNCs

For the modification of CNC films, 20 ml of 0.05 M phenylacetic acid diazonium salt (dPAA) aqueous solution and 1 ml of 0.1 M L-ascorbic acid were added onto a CNC surface for 1 h, followed by rinsing thoroughly with water. Then 5 ml 0.4 M EDC and 5 ml 0.1 M NHS were mixed, and the modified slides were incubated in the mixture for 30 min, followed by rinsing with water and blow drying with argon. The micropipette was used distribute 2 ml 670 nM goat IgG antibody (anti-g-IgG) solution evenly on the surface and let it sit for 2 h, followed by rinsing with phosphate buffer and blow it drying.

3.2.5 Infrared Spectra Measurements

All IRRAS spectra were recorded using a Mattson Infinity Fourier Transform Spectrometer (Madison, WI, USA) equipped with a low noise mercury-cadmium-tellurium (MCT) detector cooled at 77 K with liquid

nitrogen. A reflection accessory and a home-built slide holder were housed in an external auxiliary bench. A self-assembled C_{18} thiol monolayer on gold substrate was used as the background. Gold slides with CNC films before and after immersion in IgG solutions were examined. Spectra were taken using 500 scans at 2 cm^{-1} resolution with a glancing angle of 86°.

3.2.6 SPR Measurements

The CNC-based bioassays were detected using a GWC Instruments SPR imager II (Madison, WI, USA). Experiments were performed at a fixed viewing angle by a manual tuning. The interference filter produced a bandpass of 1.5 nm (FWHM) at 795 nm. Buffer and antigen solutions were introduced to the surface via a peristaltic flow through a flow cell. For analysis of antibody-antigen binding curves, the IgG antibody immobilized CNC surface was blocked with 1% BSA and LYZ mixture in PB for 1 h prior to the introduction of antigens. Each antigen solution was introduced to the array, in sequence from the lowest to the highest concentration, and flushed out with phosphate buffer after the sensorgram leveled off. The whole process was recorded in a sensorgram of the SPR intensity units vs. time. The value of %R, or Δ%R in the case of difference images, can be obtained from I_p by the following equation:[31]

$$\Delta\%R = \frac{0.85 I_p}{I_s} \times 100\% \qquad (3.1)$$

where I_p and I_s refer to the reflected light intensity detected using p- and s-polarized light, respectively. I_s gives the maximum reflectivity value at a given viewing angle, as the s-polarized radiation does not couple to surface plasmon.

3.3 Results and Discussion

3.3.1 IRRAS results of IgG immobilization on CNC films

The immobilization of antibodies to surfaces is a key step in heterogeneous immunoassay design. There are a number of methods to immobilize antibodies and other proteins to surfaces. In this work we investigate non-specific physisorption and immobilization via a covalent bond using IRRAS.

3.3.1.1 Non-specific Physisorption

IRRAS was employed to investigate the physisorption of IgG antibodies on spin-coated CNC films. The spectral results of CNC films before and after incubation in goat IgG antibody (anti-g-IgG) solutions and in blocking buffer are shown in Figure 3.03. The characteristic peaks in the region between 900 and 1500 cm^{-1} are assigned to C–O stretching and O–H in-plane bending bands for CNCs, which have been discussed in Chapter 2. The intense amide I and II peaks demonstrate a strong affinity of IgG antibodies to the CNC films. The increase in the amide peak absorbance in spectrum 3 compared with spectrum 2 indicates that the small proteins in the blocking buffer have covered the exposed CNCs, which will help to reduce non-specific adsorption.

Takahashi and coworkers also pointed out that IgG molecules have a wide range of charge diversity.[32] Therefore, absorption of IgG molecules should be influenced by electrostatic interactions.[32] Since IgG molecules have variable regions, the iso-electric point of IgG is not a unique number but a range of 6.5–8.5.[33] So the overall charge on IgGs are variable under physiological conditions. Yet due to its wide range of charge diversity, the positively charged regions of IgGs can readily adsorb to CNC surface through electrostatic forces.
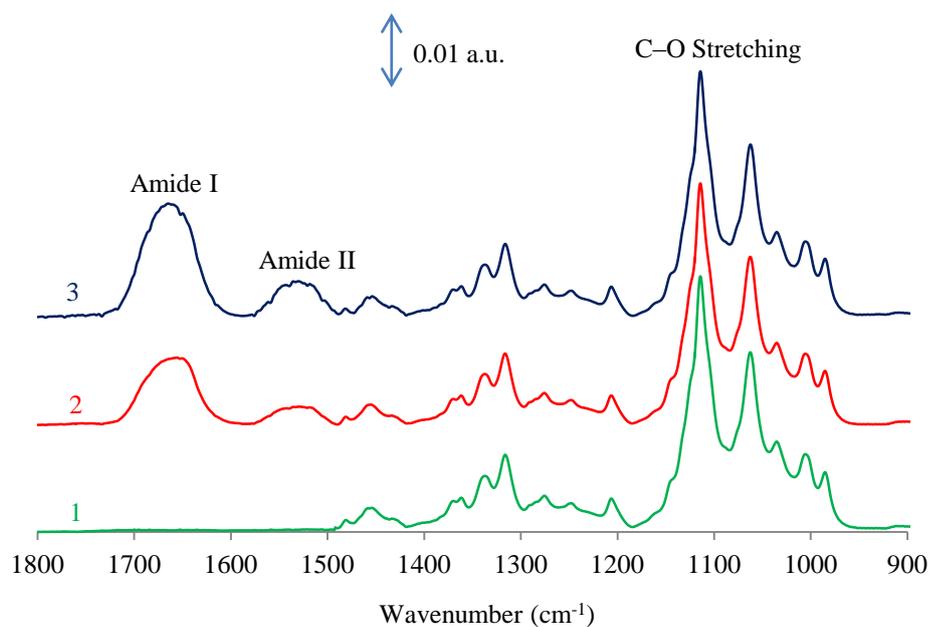

Figure 3.03. IRRAS results of physisorption of anti-g-IgGs on CNC films. Spectrum 1: original CNC films. Spectrum 2: CNC films after exposure to 670 nM anti-g-IgG solutions for 2 h. Spectrum 3: CNC films after exposure to 670 nM anti-g-IgG solutions for 2 h and blocked with blocking buffer for 1 h.

A non-specific interaction between IgGs and the CNC film is a prerequisite for IgG antibody to physically adsorb onto the CNC films. In most cases, protein adsorption has been found to be an irreversible process under physiological conditions. In our experiments, the pH, ionic strength, pressure and temperature are kept stable to minimize desorption from occurring.

3.3.1.2 Chemisorption via Covalent Bonding

The stability of an adsorbed antibody layer is a vital element in the performance of a biosensor. The potential for solvent-mediated desorption exists for non-covalent physical adsorption coatings, while covalently immobilized antibody provides a more stable means of surface immobilization.[11-13]

Phenylacetic acid diazonium salt (dPAA) is used to pre-functionalize CNC with surface carboxylic acids. Figure 3.04 shows AFM results of CNC films before and after incubation in dPAA for 10, 20 and 40 minutes. Some irregular shaped islands have formed on CNC films and the islands grow larger as the incubation time increases. The formation and growth of these islands are possibly due to the accumulation of dPAA molecules. The proposed mechanism involves the reduction of dPAA diazonium ions by ascorbic acid to form radical intermediates in close proximity to the CNC film surface.[24] The radical intermediates then bind to the surface forming the initial film. Further, it is likely that an excess of aryl radical intermediates attack already attached molecules on the surface thereby forming multilayers (Figure 3.02). [21][34]
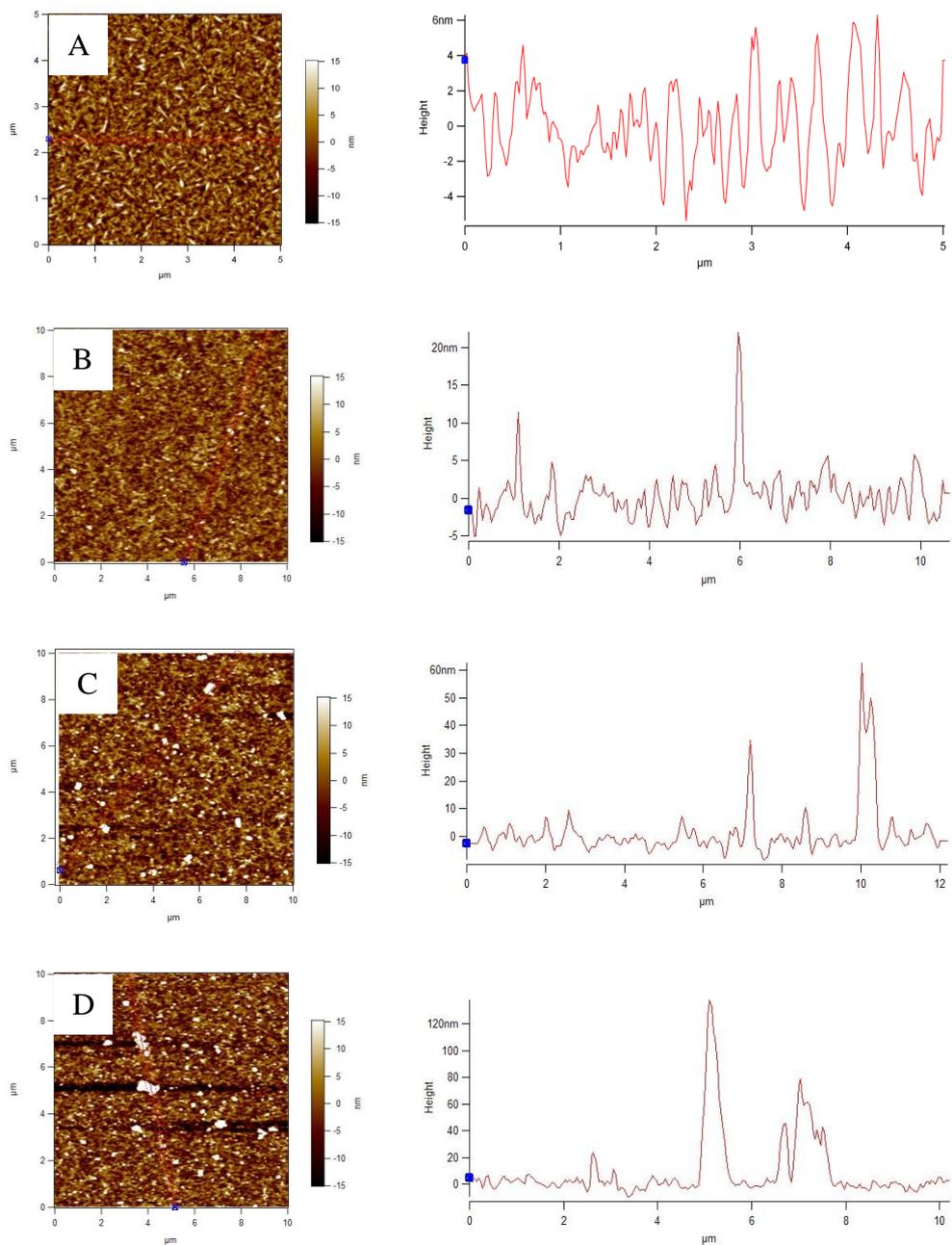
Figure 3.04. AFM images (AC mode, air) of CNC films before (A) and after (B, C and D) dPAA modification. The immersion time for CNC films in dPAA solutions for B, C and D is 10 min, 20 min and 40 min, respectively. On the right are plotted cross-sectional profiles through each of the images.

IRRAS was also used to confirm the CNC surface modification by dPAA and to probe the attachment of IgG antibodies. The antibody immobilization was achieved through covalent attachment to the NHS/EDC activated CNC surface (Figure 3.01). Spectrum 1 in Figure 3.05 illustrates the CNC surface functionalization with phenylacetic acid diazonium salt with the aid of L-ascorbic acid (Figure 3.02). In comparison with the IRRAS spectrum of CNC films, it shows many peaks characteristic of carboxylic acids and aryl rings. The band at 1715 cm^{-1} can be assigned to C=O stretch in carboxylic acid, and bands at 1607 and 1517 cm^{-1} refer to the benzene ring stretch. Both support successful modification of the CNC by dPAA. Prior to introduction of antibodies, the dPAA derived surface was activated with 0.4 M EDC and 0.1 M NHS for 30 minutes (Figure 3.01 and 3.02). In spectrum 2 of Figure 3.05, the peak at 1715 cm^{-1} in spectrum 1 has shifted to 1741 cm^{-1} in spectrum 2, which can be assigned to C=O stretch of an ester, showing the formation of the NHS ester. The strong bands at 1207 cm^{-1} (C–N–C stretch) also confirm the activation with the succinimidyl group. In addition, there is a shoulder near 1710 cm^{-1} in spectrum 2, indicating the incomplete conversion of the carboxylic acid groups to NHS esters. One of the reasons is that multilayer acid groups have been formed during the dPAA modification process, which sterically hinders the accessibility to buried acid groups. This observation is consistent with previous results which also reported the less than 100% yields of NHS esters.[15, 35] The activated surface was then used to covalently

immobilize antibodies to the surface by incubating in 670 nM anti-g-IgG solutions in phosphate buffer for 2 h, and then backfilling with blocking buffer for 1 h. The IRRAS results of these two steps are shown in spectra 3 and 4 in Figure 3.05.
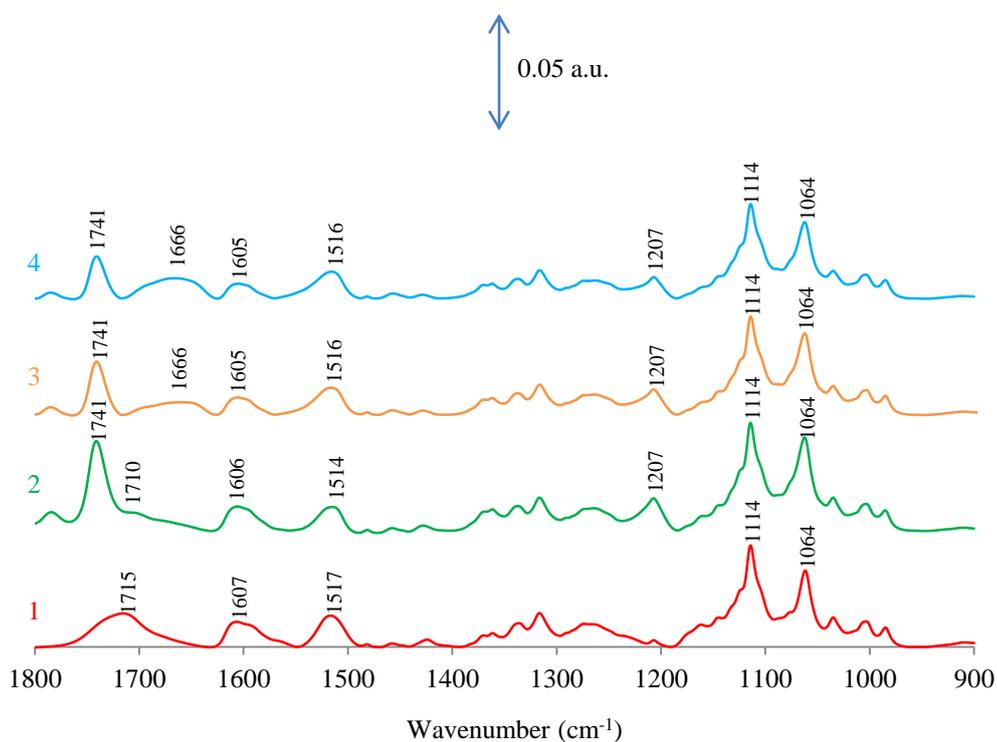
Figure 3.05. IRRAS results of chemsorption of anti-g-IgGs on phenylacetic acid (dPAA) diazonium salt modified CNC films. Spectrum 1: modification of CNC films with phenylacetic acid diazonium salt. Spectrum 2: EDC/NHS activation of dPAA modified CNC films. The activated dPAA modified CNC films exposure to 670 nM anti-g-IgG solutions for 2 h (spectrum 3) and incubated with blocking buffer for 1 h (spectrum 4).

Table 3.1. Absorbance of 1741 cm^{-1} bands for spectra 2, 3 and 4 in Figure 3.05.

Spectrum	Absorbance of bands at 1741 cm^{-1} (a.u.)
2	3.9 ($\pm$0.4) $\times$ 10^{-2}
3	2.2 ($\pm$0.8) $\times$ 10^{-2}
4	1.8 ($\pm$0.3) $\times$ 10^{-2}

The absorbance of peaks at 1741 cm^{-1} for spectra 2, 3 and 4 are listed in Table 3.1. The absorbance decreases by the addition of protein solutions, and new peaks which can be assigned to amide I bands are observed at 1666 cm^{-1} in spectra 3 and 4. This observation is accounted to the reaction of protein primary amine groups with the NHS esters, as illustrated in Figure 3.01 C. However, the 1741 cm^{-1} peak in spectrum 4 indicates that there are unreacted NHS groups that cannot be accessed by proteins.

At this point both physical and chemical antibody immobilization approaches on CNC films have been studied. A comparison of physisorption and chemisorption of antibodies onto CNC films based on IRRAS is shown in Figure 3.06. The result for antibody immobilization based on the amide I intensity as a measure of antibody coverage is shown in Table 3.2. Physisorption results in much higher surface density of antibody adsorption than chemisorption. The chemical adsorption has a relatively more complicated experimental process and reaction in each step can be incomplete, resulting in a significant reduced amount of antibody immobilized. In addition, not all of the activated NHS ester groups within the thick CNC film (~25 nm) can have protein immobilized. A normal IgG molecule has a diameter of approximately 15 nm in solution and 20-40 nm on a surface due to protein unfolding.[36] It is unlikely that such a large protein will penetrate very deep into the CNC layers to react with NHS ester groups in bottom layers. Therefore, the protein binding capacity will be highly reduced. In addition, the height of the dPAA islands formed on CNC films in chemisorption method can reach more than 100 nm, which will significantly decrease the sensitivity in surface plasmon resonance (SPR) studies. Considering all the aspects discussed above, physisorption of antibodies on CNC films is selected for the following SPR studies.
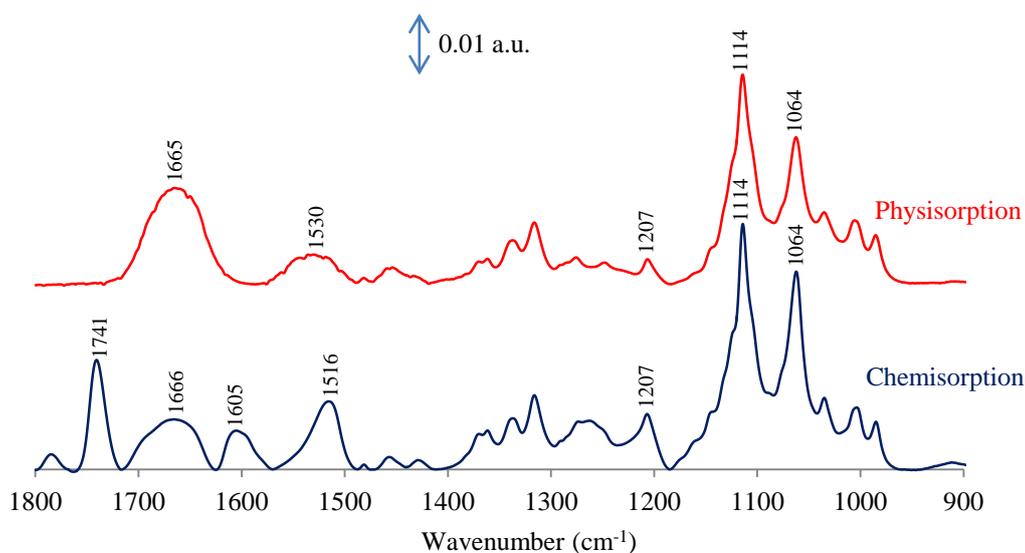
Figure 3.06. Comparison of physisorption (red spectrum) and chemsorption (blue spectrum) of anti-g-IgGs on CNC films using IRRAS.

Table 3.2. Absorbance of amide I bands for spectra 1 and 2 in Figure 3.06.

Spectrum	Absorbance of amide I bands (a.u.)
1	$1.4 \ (\pm 0.2) \times 10^{-2}$
2	$0.84 \ (\pm 0.04) \times 10^{-2}$

3.3.2 SPR-based Immunoassays Using CNC Films as a Platform

Initial attempts to observe antibody immobilization on CNC films by IRRAS have achieved success. SPR is employed to observe the dynamic events in antibody-antigen binding process.[13,37-39]

The spin coated CNC film was formed on the SPR chip and antibodies were physisorbed onto the CNC films by exposure to 670 nM anti-g-IgG solutions in phosphate buffer for 2 h. The high antibody concentration results in a high antibody surface density, which will lead to a larger observed signal.

To minimize the non-specific adsorption, a mixture of LYZ and BSA was used to block the surface prior to antigen exposures. BSA is a ubiquitous blocking agent in surface assays.[40] Drawing from the previous results in chapter 2, large amounts of LYZ can readily adsorb on dense CNC films due to electrostatic attraction. A mixture of these two small proteins is capable of covering most of the exposed CNC nanoparticles which are not bound with antibodies.

The SPR chip was incubated in phosphate buffer for 10 minutes to equilibrate prior to exposure to antigens. The performance of the antibody chip was then evaluated by flowing a series of goat IgG antigen (g-IgG) solutions from low to high concentrations and monitoring the response with SPR. The surface was then rinsed with phosphate buffer for 10 minutes to remove any unbound proteins. The whole process was recorded in a sensorgram of the SPR intensity units vs. time (sec) as shown in Figure 3.07. The SPR intensity change (I_p) can be obtained by calculating the difference between the signal after buffer rinsing and the baseline as labeled in Figure 3.07.
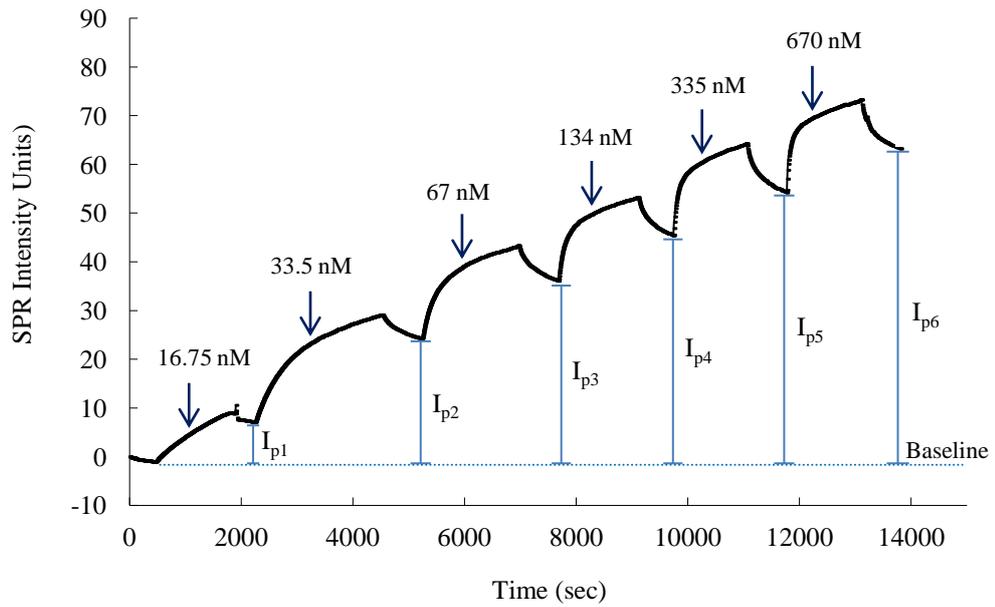
Figure 3.07. Sensorgram of SPR reflected intensity vs. time by flowing a series of goat IgG antigen (g-IgG) solutions from low to high concentrations as labeled.

The changes in percent reflectivity ($\Delta\%R$) can be calculated from the I_p values using equation 3.1. The binding curve of $\Delta\%R$ as a function of antigen concentrations was constructed as shown in Figure 3.08. The curve was fit with a one-site saturation ligand binding model using equation 3.2. This model is the same as Langmuir model. It assumes monolayer coverage, all adsorption sites are equivalent, and that the adsorbing molecules do not interact with each other.

$$\Delta\%R = \frac{\Delta\%R_{max}\ C}{K_d + C} \qquad\qquad (3.2)$$

where $\Delta\%R_{max}$ is an asymptotic saturation value obtained from the regression analysis, [C] is the concentration of protein in solution, and K_d is the dissociation constant. As K_a and K_d values are typically ascribed to solution based measurements we will refer to these values as K_{ads} and K_{ads}^{-1}, a more physically correct nomenclature for surface based bioassays.[41] In our study the adsorption constant K_{ads}, which is the reciprocal of the K_d value ($K_{ads} = 1/K_d$), will be reported and is characteristic of the adsorption strength. All the fitting parameters are listed in Table 3.3.

Figure 3.08 shows that the amount of adsorbed g-IgGs increases sharply at low concentrations and reaches a plateau at approximately 200 nM. It has been shown for constant angle SPR imaging that $\Delta\%R$ is linear with surface concentration when $\Delta\%R$ is 10-20% or less.[42, 43] Although the magnitude of $\Delta\%R$ at the spot of 670 nM g-IgG slightly exceeds 20%, the trend of the isotherm that the amount of captured antigens increases with the concentration of antigen solutions is valid. The K_{ads} value determined from the isotherm fitting is 1.8 ($\pm$0.4) $\times$ 10^7, which can be used to compare to K_{ads} values in similar systems.[41] Comparison of the K_{ads} value with other values obtained using different surface chemistry[31,44] shows no significant differences with values in the low 10^7 M^{-1} range.
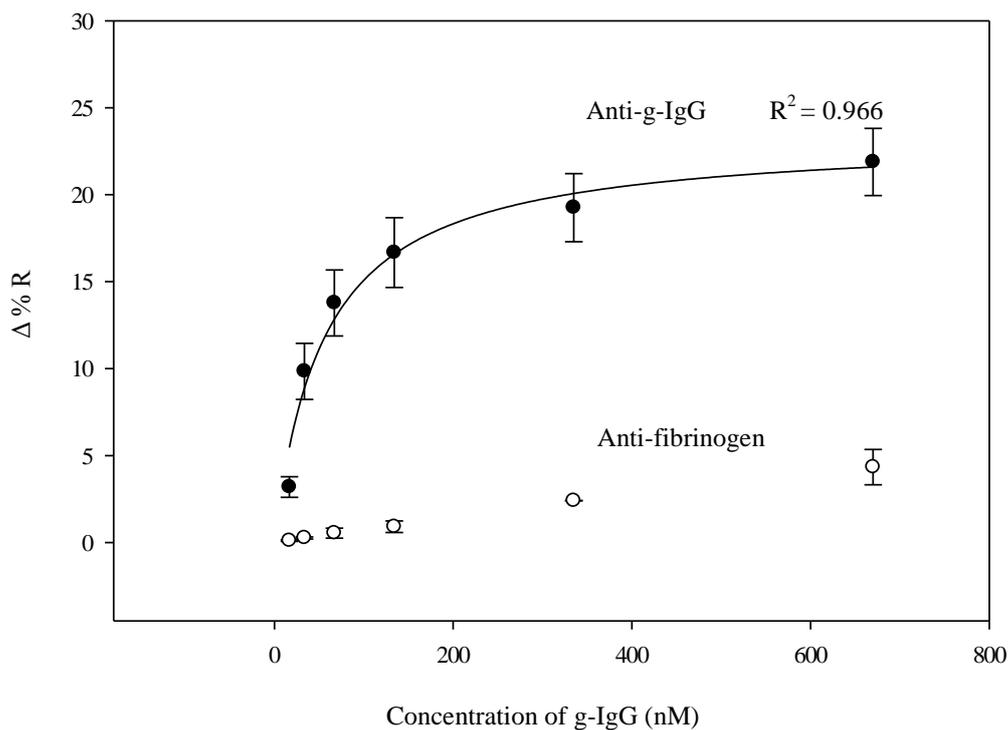
Figure 3.08. The circles are the data points and the lines through the data are both fitted with a one-site saturation ligand binding model. (Filled circles) Binding curve of g-IgGs with anti-g-IgGs that are physisorbed on spin coated CNC films. The control group (open circles) describes the non-specific binding of g-IgGs with CNC films adsorbed by anti-fibrinogens. The error bars represent the standard deviation of the mean for a minimum of 2 separate bioassays.

Table 3.3. Curve fitting parameters using a one site saturation ligand binding model for the antigen binding curve obtained by SPR on spin coated CNCs that are physisorbed with anti-g-IgGs

R^2	K_{ads} (M^{-1})	$\Delta\%R_{max}$
0.966	$1.8 (\pm 0.4) \times 10^7$	23 ± 1

A control experiment to measure nonspecific adsorption was conducted using physisorbed anti-fibrinogen and the same g-IgG sample solutions. The binding curve for the non-specific binding is also shown in Figure 3.08. Compared with the binding of anti-g-IgG and its complementary antigen, signals due to non-specific adsorption are very low. It suggests that the nonspecific interaction will not have much effect on the assay.
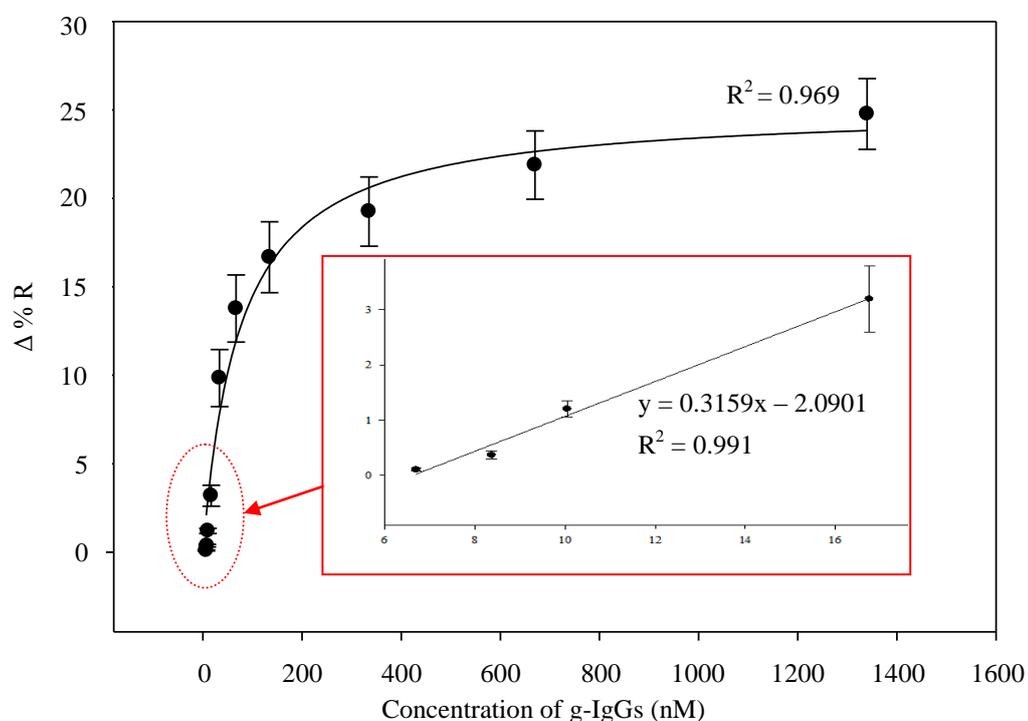
*Figure 3.09*. Binding curve of g-IgGs with anti-g-IgGs that are physisorbed on spin coated CNC films. The circles are the data points and the line through the data is fitted with a one-site saturation ligand binding model. The magnified area highlights the lower end of the concentration range and fitted using a linear least squares analysis. The error bars represent the standard deviation of the mean for a minimum of 2 separate bioassays.

To determine the limit of detection (LOD) for the CNC-based bioassay, a series of g-IgG solutions with low concentrations were also run and the data points were added to the binding curve, which is illustrated in Figure 3.09. The magnified area in the figure highlights the lower end of the concentration range and is fitted using a linear least squares analysis

$$LOD = 3\sigma_{blank} + blank$$

(3.3)

According to equation 3.3, the LOD can be approximately obtained by three times the standard deviation of the background plus the signal for blank. When buffer is flowed through, the signal is zero. By converting this value to a concentration using the linear fit obtained from least squares analysis shown in Figure 3.09, the instrumentally limited LOD is calculated to be 7.0 (±1.3) nM. It is understood that in these types of assays non-specific adsorption as measured by the control experiment will govern the LOD. So if using the signal detected for 16.75 nM in the control group for the blank, and by converting the value to a concentration using the linear fit in Figure 3.09, the LOD is calculated to be 17 (±3) nM. The error was determined by propagating the error associated with the blank measurement through calculations. Though it may not be the lowest LOD reported for surface based immunoassays,[45,46] the CNC films still successfully provide a platform for immunoassays. Since it has shown that the affinity between immobilized antibodies and their antigens

increases at high surface density[1], it is expected that antigens bind more readily on antibody adsorbed CNC films.

3.4 Conclusion

The work presented in this chapter looked at using CNC films as a platform for immunoassays and a detailed investigation on the impact of antibody immobilization chemistry on assay performance was presented. A new method of functionalizing CNC films by phenylacetic acid diazonium salt (dPAA) using ascorbic acid was reported. AFM and IRRAS results confirmed the surface functionalization of CNC films with carboxylic acids. Antibody immobilization was achieved through non-specific adsorption and through covalent attachment to the NHS/EDC activated CNC surface. Based on IRRAS results, antibody immobilization through physical adsorption provided a substrate with higher surface density of antibody compared to the performance of covalent attachment. The CNC-based immunoassay with physisorbed antibodies was further evaluated by SPR, which confirmed the ability of the immunoassay to detect antigen binding with an instrumental LOD of 7.0 ($\pm$1.3) nM and a non-specific adsorption governed LOD of 17 ($\pm$3) nM.

3.5 References

1. Giraudi, G.; Rosso, I.; Baggiani, C.; Giovannoli, C. *Analytica Chimica Acta* **1999**, *381*, 133–146.

2. Haynes, C. A.; Norde, W. *Colloids and Surfaces B: Biointerfaces* **1994**, *2*, 517–566.

3. Hlady, V.; Buijs, J. *Current Opinion in Biotechnology* **1996**, *7*, 72–77.

4. MacBeath, G.; Schreiber, S. L. *Science* **2000**, *289*, 1760–1763.

5. Ng, H. T.; Fang, A.; Huang, L.; Li, S. F. Y. *Langmuir* **2002**, *18*, 6324–6329.

6. Levit-Binnun, N.; Lindner, A. B.; Zik, O.; Eshhar, Z.; Moses, E. *Analytical Chemistry* **2003**, *75*, 1436–1441.

7. Chibata, I. (1978) Immobilized Enzymes – Research and Development Chap. 2 (John Wiley, New York).

8. Ball, V.; Huetz, P.; Elaissari, A.; Cazenave, J.; Voegel, J.; Schaff, P. *Proceedings of the National Academy of Sciences* **1994**, *91*, 7330–7334.

9. Lutanie, E.; Voegel, J.; Schaff, P. Freund, M.; Cazenave, J.; Schmitt, A. *Proceedings of the National Academy of Sciences* **1992**, *89*, 9890–9894.

10. Lundstrom, I. *Biosensors and Bioelectronics* **1994**, *9*, 725–736.

11. Carome, E. F.; Coghlan, G. A.; Sukenik, C. N.; Zull, J. E. *Sensors and Actuators B*: *Chemical* **1993**, *14*, 732–733.

12. Lofas, S.; Johnsson, B. *J. Chem. Soc. Chem. Comm.* **1990**, 1526–1528.

13. Disley, D. M.; Cullen, D. C.; You, H. X.; Lowe, C. R. *Biosensors and Bioelectronics* **1998**, *13*, 1213–1225.

14. Parker, M.-C.; Davies, M. C.; Tendler, S. J. B. *Journal of Applied Physics* **1995**, *99*, 16155.

15. Frey, B. L.; Corn R. M.; *Analytical Chemistry* **1996**, *68*, 3197–3193.

16. Wagner, P.; Hengner, M.; Kernen, P.; Zaugg, F.; Semenza, G. *Biophysical Journal* **1996**, *70*, 2052.

17. Hermanson, G. T. (2008) Bioconjugate Techniques, 2nd ed., Academic Press: Amsterdam,

18. Delamar, M.; Hitmi, R.; Pinson, J.; Saveant, J. M. *Journal of the American Chemical Society* **1992,** *114 (14)*, 5883–5884.

19. Allongue, P.; Delamar, M.; Desbat, B.; Fagebaume, O.; Hitmi, R.; Pinson, J.; Saveant, J. M. *Journal of the American Chemical Society* **1997,** *119 (1)*, 201–207.

20. Delamar, M.; Desarmot, G.; Fagebaume, O.; Hitmi, R.; Pinson, J.; Saveant, J. M. *Carbon* **1997,** *35 (6)*, 801–807.

21. Kariuki, J. K.; McDermott, M. T. *Langmuir* **2001,** *17 (19)*, 5947–5951.

22. Liu, Y. C.; Mccreery, R. L. *Journal of the American Chemical Society* **1995,** *117 (45)*, 11254–11259.

23. Anariba, F.; DuVall, S. H.; McCreery, R. L. *Analytical Chemistry* **2003,** *75 (15)*, 3837–3844.

24. Pinson, J.; Podvorica, F. *Chemical Society Reviews* **2005,** *34 (5)*, 429–439.

25. Laurentius, L., Stoyanov, S. R., Guserov, S., Kovalenko, A., Du, R., Lopinski G, P., McDermott, M. T. *ACS Nano* **2011**, *5*, 4219–4227.

26. Du, R.; McDermott, M. T. manuscript in preparation.

27. Janeway, C. A.; Jr, P. T. Walport, M.; Shlomchik, M. J., (2001) Immunobiology. 5th ed.; Garland Science: New York,

28. Klenkar, G.; Liedberg, B. *Analytical and Bioanalytical Chemistry* **2008**, *391*, 1679–1688.

29. Kim, S. J.; Gobi, K. V.; Tanaka, H.; Shoyama, Y.; Miura, N. *Sensors and Actuators B: Chemical* **2008**, *130*, 281–289.

30. Ratner, D. M.; Adams, E. W.; Su, J.; O'Keefe, B. R.; Mrksich, M.; Seeberger, P. H. *ChemBioChem* **2004**, *5 (3)*, 379–383.

31. Kanda, V.; Kariuki, J. K.; Harrison, D. J.; McDermott, M.T. *Analytical Chemistry* **2004**, *76*, 7257–7262.

32. Takahashi, S.; Wada, N.; Harada, K.; Nagata, M. *Kidney International* **2004** *66*, 1556–1560.

33. Kane, M. M.; Banks, J. N. (2000). In *Immunoassays* Gosling JP (ed), chapter 2, 52–53, Oxford University Press, Oxford.

34. Kariuki, J. K.; McDermott, M. T. *Langmuir* **1999,** *15 (19)*, 6534-6540.

35. Shang, H. PhD thesis, Department of Chemistry, University of Alberta, 2008.

36. Ouerghi, O.; Touhami, A.; Othmane, A.; Ouada, H. B.; Martelet, C.; Fretigny, C.; Jaffrezic-Renault, N. *Biomolecular Engineering* **2002**, *19*, 183−188.

37. Klonisch, T.; Panayotou, G.; Edwards, P.; Jackson, A. M.; Berger, P.; Delves, P. J.; Lund, T.; Roitt, I. M. *Immunology* **1996**, *89*, 165−171.

38. Bae, Y. M.; Oh, B.-K.; Lee, W.; H.; Choi, J.-W. *Biosensors and Bioelectronics* **2005**, *21*, 103−110.

39. Chen, S.; Liu, L.; Zhou, J.; Jiang, S. *Langmuir* **2003**, *19*, 2859−2864.

40. Christofides, N. D. In the Immunoassay Handbook, 2nd ed.; Wild, D. Ed.; Nature Publishing Group: New York, 2001, pp 61−77.

41. Smith, E. A.; Thomas, W. D.; Kiessling, L. L.; Corn, R. M. *Journal of the American Chemical Society* **2003**, *125*, 6140−6148.

42. Shumaker-Parry, J. S.; Campbell, C. T. *Analytical Chemistry* **2004**, *76*, 907−917.

43. Nelson, B. P.; Grimsrud, T. E.; Liles, M. R.; Goodman, R. M.; Corn, R. M. *Analytical Chemistry* **2001**, *73*, 1−7.

44. Toman, T. J. MSc thesis, Department of Chemistry, University of Alberta, **2013**.

45. Cao, C.; Sim, S. J. *Biosensors and Bioelectronics* **2007**, *22*, 1874−1880.

46. Grant, C. F. PhD thesis, Department of Chemistry, University of Alberta, **2009**.

Chapter 4 Conclusion and Future Work

4.1 Conclusion

This thesis has for the first time studied the effect of cellulose nanocrystal (CNC) films on protein adsorption to evaluate new biosensing substrates. The work presented in Chapter 2 detailed the formation and characterization of, and studied the interactions between CNC films and a variety of proteins (bovine fibrinogen, bovine serum albumin and chicken lysozyme) by infrared reflection absorption spectroscopy (IRRAS) and atomic force microscopy (AFM). Both spontaneous and spin coating processes were used to form a uniform CNC film via physisorption to an amine-terminated thiol layer on gold. The CNC film thickness was well controlled by the CNC suspension concentration. The spin coating produced a much thicker film which could be as thick as 50 nm when using 3 wt% CNC suspensions.

Both of the films were utilized for CNC-protein interaction studies. CNC films do not generally inhibit protein adsorption as we expected. The major driving force responsible for the interaction between proteins and CNC films is electrostatic in nature due to the negatively charged CNC surface. The amount of protein adsorption highly depends on the iso-electric point of the proteins. CNC films have a strong interaction with cationic proteins such as lysozyme, while exhibiting weak affinity for anionic proteins such as bovine serum albumin. Other factors that influence the protein adsorption on CNC

films include protein molecular weight and charge distribution.

In addition, the thin CNC films prepared by immersion contain gaps in the CNC network, resulting in the exposed ammonium/amine groups also contribute to the non-specific protein adsorption. This unwanted protein adsorption to exposed ammonium/amine groups can be prevented by using thicker spin coated CNC films. Comparing the protein adsorption on CNC films prepared by immersion, LYZ adsorption on spin coated CNC films increased significantly while the BSA adsorption was inhibited, which further confirms that electrostatic forces play a key role in interactions between CNC film and proteins.

A thorough understanding of protein adsorption has laid the foundation for the use of CNC films in biosensing applications. In Chapter 3 a CNC film based immunoassays was developed and evaluated. Both physisorbed and covalently bonded IgG antibodies were studied on spin coated CNC films. Importantly, we reported a novel method to modify CNC surfaces with phenylacetic acid diazonium salt imparting a carboxylic acid terminated surface to the CNC films. The diazonium salt reduction was carried out with the addition of a reducing agent L-ascorbic acid to form radical intermediates that can bind to the CNC surface. Antibodies can then covalently attach to NHS activated CNC films which were pre-functionalized by phenylacetic acid diazonium salt. Compared to the performance of covalent attachment, antibody immobilization through physical adsorption provided a substrate with

higher surface density of antibody, indicating the CNC functionalization process needs to be further optimized. The CNC-based immunoassay with physisorbed antibodies was further evaluated by SPR, which confirmed the ability of the immunoassay to detect antigen binding with a detection limit of 17 (±3) nM.

Overall, the proposed platform based on CNC films with physisorbed IgG proteins is expected to open new pathways for deployment in new CNC applications such as drug delivery, biodetection, filtration of pathogens, and bio-sensing platforms that utilize green-material substrates. At present, nanoscience and nanotechnology are disciplines that have been highlighted for special focus by many funding agencies and government strategies. Many novel products have been created and further developed with the help of nanotechnology. Undoubtedly, the exploitation of CNC will become a bridge between nanoscience and natural resource products, which could play a major role in reviving the forest industry in Canada and countries with abundant forest resources.

4.2 Future Work

The immobilization of proteins is important for practical processes and analytical applications based on the specificity of biochemical recognition. Commonly, proteins are immobilized on hard substrates, such as glass, silica, metals or magnetic particles. [1] However, a major problem in protein

immobilization is the preservation of the native conformation and activity of proteins on the solid support.[2] The use of natural polymers as a support has received considerable attention because of their high biocompatibility.[3] CNC as a natural polymer has the potential to preserve the native conformation and activity of proteins. Therefore, investigating the interaction between CNC nanoparticles and proteins in an aqueous environment is expected to be useful for preparing protein-based functional materials for industrial and biomedical purposes.

Some important information can be drawn from previous studies on interactions between polysaccharides and proteins.[4,5] A series of forces are dominant in the interactions of polysaccharide and protein complexes in aqueous solutions, such as hydrogen bonding[6], hydrophobic interactions[7], electrostatic interactions [8] and repulsive interactions[9]. Drawn from our conclusion, the interaction between CNCs and proteins is dominantly driven by electrostatic forces. Besides the parameters that influence the interactions between proteins and CNC films including pH, molecular weight, iso-electric point and protein concentration, CNC-protein ratio should be another important factor that influences the CNC-protein interactions in aqueous solutions. A maximum protein adsorption yield is obtained for a specific ratio for each system. Schmitt et al. have shown that the specific ratio for the formation of complexes between acacia gum and h-lactoglobulin is 1:4.[10] A wide variety of techniques have been used for studying polysaccharide-protein

interactions, such as UV-vis[11], fluorescence[12] and zeta potential[13]. They are all applicable to further studies on the interaction of CNCs with proteins in suspensions.

Furthermore, the functionalization of CNC surface needs to be optimized. Though the AFM and IRRAS results show successful modification of CNC films with phenylacetic acid diazonium salt (dPAA), some important information on the functionalization, such as the dPAA attachment mechanism and binding site, needs to be determined. In addition, it was noticed that irregular shaped islands, which are probably due to the accumulation of dPAA molecules, have formed on CNC films. A new method of preparing a smooth CNC film with terminal carboxylic acid groups needs to be developed for further SPR studies.

4.3 References

1. Caygill, R. L.; Blair, G. E.; Millner, P. A. *Analytica Chimica Acta* **2010**, *681*, 8–15.

2. Kiyonaka, S.; Sada, K.; Yoshimura, I.; Shinkai, S.; Kato, N.; Hamachi, I. *Nature Materials* **2004**, *3*, 58–64.

3. Isobe, N.; Lee, D.-S.; Kwon, Y.-J.; Kimura, S.; Kuga, S.; Wada, M.; Kim, U.-J. *Cellulose* **2011**, *18(5)*, 1251–1256.

4. Imeson, A. P.; Ledward, D. **A.;** Mitchell, J. R. *Journal* of the *Science* of *Food and Agriculture* **1977***, 28***,** 661–668.

5. Imeson, A. P. (1984) Recovery and utilisation of proteins using alginate. In Gums and Stabilisers for the Food Industry 2, pp 189. (Applications of Hydrocolloids; Phillips, G.O., Wedlock, D.J., Williams, P.A., Eds.) Oxford: Pergamon Press.

6. Louisot, P. (1989) Biochimie Generale et Medicale, pp 488, SIMEP, Paris.

7. Taravel, M. N.; Domard, A. *Biomaterials* **1995**, *16*, 865–871.

8. Ambjerb Pedersen, H.C.; Jorgensen, B.B. *Food Hydrocolloids* **1991**, *5*, 323-328.

9. Polyakov, V.I.; Grinberg, V.Y.; Tolstoguzov, V.B. *Food Hydrocolloids* **1997**, *11*, 171–180.

10. Schmitt, C.; Sanchez, C.; Desorbry-Banon, S.; Hardy, J. *Critical* Reviews in *Food Science* and *Nutrition* **1998**, *38*, 689–753.

11. Liu, H.; Zhu, J. Y.; Chai, X. S. *Langmuir* **2011**, *27(1)*, 272–278.

12. Hong, J.; Ye, X.; Zhang, Y.-H. P. *Langmuir* **2007,** *23(25),* 12535–12540.

13. Paquot, M.; Godin, F.; Dumont de Chassart, Q. *LWT - Food Science and Technology* **1994**, *27(1)*, 11–15.